

# How Spatially Modulated Activity Reshapes Active Polymer Conformations

Paolo Malgaretti<sup>1,\*</sup> and Emanuele Locatelli<sup>2,3</sup>

<sup>1</sup> *Helmholtz Institute Erlangen-Nürnberg for Renewable Energy (IET-2),  
Forschungszentrum Jülich, Cauerstr. 1, 91058 Erlangen, Germany*

<sup>2</sup> *Department of Physics and Astronomy, University of Padova, Via Marzolo 8, I-35131 Padova, Italy*

<sup>3</sup> *INFN, Sezione di Padova, Via Marzolo 8, I-35131 Padova, Italy*

Active polymers are driven out of equilibrium by internal forces and exhibit conformational properties that differ fundamentally from those of passive chains. Here we study how spatially modulated tangential activity reshapes the conformations of semiflexible polymers. Using a continuum Rouse model with bending rigidity, we develop a systematic expansion in the limit of weak activity and derive analytical expressions for mode correlations, gyration radius, and end-to-end distance under sinusoidally varying propulsion. We show that spatially structured activity breaks self-similar scaling and induces a mode-dependent transition between polymer shrinking and swelling. Uniform or low-mode forcing produces compact, globule-like conformations, whereas higher modes generate alternating stretched and compressed segments, leading to globally swollen chains. Different polymer sizes respond differently to activity, allowing for conformations that are compact in gyration radius yet extended in end-to-end distance. Langevin dynamics simulations quantitatively confirm the theoretical predictions. Our results demonstrate that even weak, patterned activity provides a powerful mechanism to control polymer conformations far from equilibrium.

## I. INTRODUCTION

Active systems are characterized by their ability to break equilibrium at the local scale. This disruption leads to the emergence of dynamical and collective properties that are strikingly different from their equilibrium counterparts or even those of externally driven systems [1]. For such reason, they have been the subject of intense study for more than two decades. Examples include Motility-Induced Phase Separation (MIPS) [2], activity-driven microphase separation in continuum models [3], giant number fluctuations [4], active turbulence [5], self-organisation phenomena [6], and flocking phases [7].

Within active systems, those composed of filamentous units have recently risen in popularity because of their relevance in biological systems, spanning different length scales from the cellular level to the macro-scale. For example, the cytoskeleton and the intracellular trafficking network, powered by molecular motors, serve diverse purposes [8, 9]. Activity is also relevant in chromatin dynamics at the level of the whole nucleus [10, 11], for interphase organisation [12, 13] with connections to experimental evidence [14], and during replication [15]. At larger scales, cilia arrays, flagella, cyanobacteria and worms are examples of filamentous systems that consume energy to perform some form of directed motion [16–22]. Further, active filaments are relevant beyond biological systems, with recent technological progress opening new frontiers for applications, such as artificial active flagella [23–27], chains made of chemically active droplets [28, 29], and soft robotic systems [30, 31].

Inspired by these diverse examples, researchers have dedicated significant attention to the characterisation of simple active polymer models. Typically, an active polymer is a chain of “active” monomers, each capable of generating force and performing autonomous motion [32]. In this study, we focus on the case of tangential or polar propulsion, where forces are oriented along the local tangent of the polymer backbone [32–34]. From a biophysical perspective, this model mimics the action of molecular motors on biofilaments such as actin or microtubules under certain conditions [8, 35]. Moreover, it represents a minimal model for the locomotive mechanism employed by filamentous bacteria or worms, where propulsion occurs via segment contraction or lateral protrusions [21].

It is interesting to note that, in three dimensions, simulations of tangentially active polymers show the emergence of a globule-like phase at high activity when the magnitude of the active forces is constant along the chain [32]; such a phase was not predicted in analytical models that do not fix the force magnitude along the polymer. Indeed, this feature makes the model nonlinear and poses a formidable challenge from an analytical perspective. In previous work [34], we introduced a set of approximations that highlighted the emergence of a more compact phase, in agreement with numerical results.

---

\*Corresponding Author : p.malgaretti@fz-juelich.de

In this work, we take on the problem from a different angle: by considering a generalized Rouse model, we perform a systematic expansion at small active forces, obtaining analytical expressions for quantities such as the gyration radius and the magnitude of the end-to-end vector. We then compare these predictions with numerical simulations for a sinusoidal activation profile (“single mode” forcing).

Even though, due to signal-to-noise ratio issues, we could not reach the small values of the active force required by the expansion, our numerical results performed for finite values of the active force confirm the predictions of our model. This shows an interesting robustness of our mode even at finite values of the active force.

## II. CONTINUUM MODEL

We model the active polymer via a Rouse model with a finite bending rigidity, as introduced in Ref. [34]:

$$\dot{\mathbf{r}}(s, t) = -\mu G \partial_s^4 \mathbf{r}(s, t) + \mu D \partial_s^2 \mathbf{r}(s, t) + \mu f(s) \frac{\partial_s \mathbf{r}(s, t)}{|\partial_s \mathbf{r}(s, t)|} + \boldsymbol{\eta}(s, t) \quad (1)$$

where  $s$  is the coordinate along the contour,  $\mu$  is the mobility of the monomers and  $\boldsymbol{\eta}$  is a white noise

$$\langle \boldsymbol{\eta}(s, t) \rangle = 0 \quad (2)$$

$$\langle \eta_i(s, t) \eta_j(s', t') \rangle = 2\mu k_B T \delta_{ij} \delta(t - t') \delta(s - s') \quad (3)$$

delta correlated in time and space. The parameters  $D$  and  $G$  are related to the monomer size,  $b$ , and polymer dimensionless persistence length,  $l_p$ , as

$$D = \frac{d k_B T}{2 b^2 l_p}, \quad G = \frac{d k_B T}{2 b^2} l_p, \quad l_p = \sqrt{G/D} \quad (4)$$

where  $d$  is the dimension of the space the polymer is embedded in; we recall that, in this framework,  $l_p \in [1 : L_0]$ ,  $L_0 = Nb$  being the contour length of the polymer. At variance with Ref. [34], the tangential active force  $f(s)$  is not necessarily constant along the contour and is, for the moment, not further specified; however, it is still characterized by a typical magnitude, dubbed  $f^a$ ; see Fig. 1a) for a sketch of the model.

Equation (1) should be completed with a set of boundary conditions (applied without the noise [36, 37]); for the case of free ends, that is, no forces on the head and tail of the polymer, the boundary conditions read [36]:

$$[D \partial_s \mathbf{r}(s, t) - G \partial_s^3 \mathbf{r}(s, t)]_{s=\pm N/2} = 0 \quad (5)$$

$$[D_0 \partial_s \mathbf{r}(s, t) \pm G \partial_s^2 \mathbf{r}(s, t)]_{s=\pm N/2} = 0 \quad (6)$$

with  $D_0 = D l_p$ . Notice that Eq. (5) is equivalent to request that

$$\dot{\mathbf{r}}_{CM}(t) = \frac{1}{N} \int_{-\frac{N}{2}}^{\frac{N}{2}} \dot{\mathbf{r}}(t) ds = \frac{1}{N} \int_{-\frac{N}{2}}^{\frac{N}{2}} \mu f(s) \frac{\partial_s \mathbf{r}(s, t)}{|\partial_s \mathbf{r}(s, t)|} ds + \frac{1}{N} \int_{-\frac{N}{2}}^{\frac{N}{2}} \boldsymbol{\eta}(s, t) ds \quad (7)$$

that is, that the dynamics of the center of mass is governed by the net force on the polymer. As explained in full detail later on and in Appendix A 1, it is necessary to introduce a finite bending rigidity to enforce the finiteness of the denominator in Eq. (7). In fact, as already discussed in Ref.[34], a small but finite bending rigidity identifies a cutoff mode  $n_p = \frac{l_p}{b} = \sqrt{\frac{G}{D b^2}}$  above which the amplitudes of modes decay as  $n^{-4}$  hence enforcing the convergence of the denominator.

### A. Eigenfunction representation

In order to get analytical insight into Eq. (3), usually one seeks the eigenfunctions of the operator on the right hand side of Eq. (3) that are compatible with the boundary conditions, Eqs. (5),(6); for the case under study, this is a formidable task. In order to avoid this difficulty, we represent the solution of Eq.(1) with the boundary conditions Eqs. (5), (6) using the eigenfunctions of the passive case,  $f^a = 0$ . We recall that this base is complete and orthonormal [36]. Accordingly, we represent:

$$\mathbf{r}(s, t) = \sum_{n=0}^{\infty} \mathbf{r}_n(t) \psi_n(s) \quad f(s) = \sum_{n=0}^{\infty} f_n \psi_n(s) \quad \boldsymbol{\eta}(s, t) = \sum_{n=0}^{\infty} \boldsymbol{\eta}_n(t) \psi_n(s) \quad (8)$$

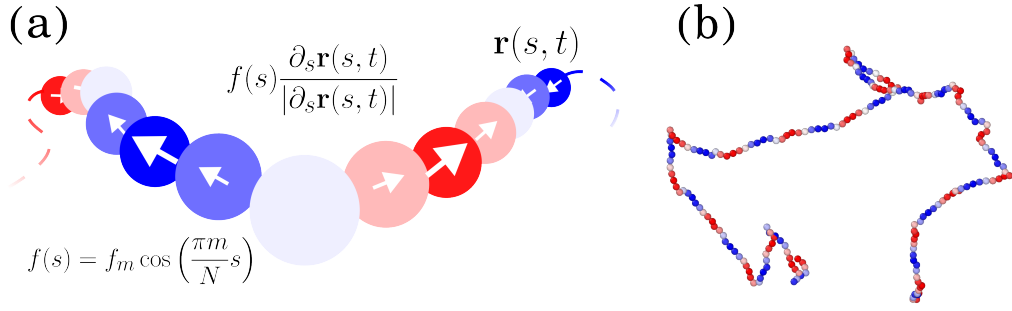


FIG. 1: (a) Sketch of the continuum active polymer  $\mathbf{r}(s, t)$ . The self-propulsion direction is modulated along the backbone as  $\cos(\pi m s/N)$  with  $s$  the coordinate along the contour of the polymer,  $N$  is the degree of polymerization and  $m$  an integer; we name this “single-mode force” and we highlight the modulation through the verse and size of the arrows. (b) Example snapshot from numerical simulations (see Sec. III) with  $m = 40$ ; colors and other parameters as in Fig.s 4, 5.

where  $r_n(t), \eta_n(t)$  are real functions and

$$\langle \eta_n(t) \rangle = 0 \quad \langle \eta_{n,i}(t) \eta_{m,j}(t') \rangle = 2\mu k_B T \delta_{ij} \delta_{n,m} \delta(t - t') \quad (9)$$

The eigenfunctions are solution of

$$-\mu G \partial_s^4 \psi_n(s) + \mu D \partial_s^2 \psi_n(s) = -\zeta_n \quad (10)$$

and read

$$\psi_0 = \sqrt{\frac{1}{N}} \quad (11a)$$

$$\psi(s)_n = \sqrt{\frac{c_n}{N}} \begin{cases} k_n \frac{\sin(k_n s)}{\cos(k_n N/2)} + \beta_n \frac{\sinh(\beta_n s)}{\cosh(\beta_n N/2)}, & l \text{ odd} \\ -k_n \frac{\cos(k_n s)}{\sin(k_n N/2)} + \beta_n \frac{\cosh(\beta_n s)}{\sinh(\beta_n N/2)}, & l \text{ even} \end{cases} \quad (11b)$$

where  $c_n$  is the normalization constant and  $k_n$  and  $\beta_n$  are determined by solving

$$\begin{aligned} k_n^3 \sin(k_n N/2) \cosh(\beta_n N/2) - \beta_n^3 \cos(k_n N/2) \sinh(\beta_n N/2) - 2p(k_n^2 + \beta_n^2) \cos(k_n N/2) \cosh(\beta_n N/2) &= 0, n \text{ odd}, \\ k_n^3 \cos(k_n N/2) \sinh(\beta_n N/2) - \beta_n^3 \sin(k_n N/2) \cosh(\beta_n N/2) + 2p(k_n^2 + \beta_n^2) \sin(k_n N/2) \sinh(\beta_n N/2) &= 0, n \text{ even}. \end{aligned} \quad (12)$$

Together with the constraint imposed by the boundary conditions  $\beta_n^2 - k_n^2 = \frac{1}{l_p^2}$  the eigenvalues are

$$\zeta_n = \mu k_n^2 (G k_n^2 + D). \quad (13)$$

Accordingly, we rewrite Eq.(1) in its eigenfunctions representation:

$$\sum_{n=0}^{\infty} \dot{\mathbf{r}}_n(t) \psi_n(s) = - \sum_{n=0}^{\infty} \zeta_n \mathbf{r}_n(t) \psi_n(s) + \frac{\sum_{n=0}^{\infty} \sum_{m=0}^{\infty} \mu f_m \mathbf{r}_n(t) \psi_m(s) \partial_s \psi_n(s)}{\sqrt{\sum_{m=0}^{\infty} \mathbf{r}_m \partial_s \psi_m(s) \cdot \sum_{n=0}^{\infty} \mathbf{r}_n \partial_s \psi_n(s)}} + \sum_{n=0}^{\infty} \boldsymbol{\eta}_n(t) \psi_n(s) \quad (14)$$

by multiplying both sides by  $\psi_i(s)$  and integrating in  $ds$  we obtain:

$$\dot{\mathbf{r}}_i(t) = -\zeta_i \mathbf{r}_i(t) + \mu \int_{-\frac{N}{2}}^{\frac{N}{2}} \frac{\sum_{n=0}^{\infty} \sum_{m=0}^{\infty} f_m \mathbf{r}_n(t) \psi_m(s) \partial_s \psi_n(s)}{\sqrt{\sum_{m=0}^{\infty} \mathbf{r}_m \partial_s \psi_m(s) \cdot \sum_{n=0}^{\infty} \mathbf{r}_n \partial_s \psi_n(s)}} \psi_i(s) ds + \boldsymbol{\eta}_i(t) \quad (15)$$

## B. Steady state correlations

We are interested in deriving closed formulas for the magnitude of the gyration radius,  $\mathcal{R}_G^2$  and the end-to-end square distance,  $\mathcal{R}_E^2$  at steady state which are functions of expectation values of the modes

$$\langle \mathbf{r}_i(t) \cdot \mathbf{r}_j(t) \rangle^{\infty} = \lim_{t \rightarrow \infty} \langle \mathbf{r}_i(t) \cdot \mathbf{r}_j(t) \rangle. \quad (16)$$

We remark that we need to compute the cross correlation among modes, since the base functions we are using, Eqs. (11), are not the eigenfunction of the time evolution operator (i.e., the right hand side of Eq. (1)). In order to derive the expressions for  $\langle \mathbf{r}_i(t) \cdot \mathbf{r}_j(t) \rangle$  at steady state, that we name  $\langle \mathbf{r}_i(t) \cdot \mathbf{r}_j(t) \rangle^\infty$ , we write first the time evolution of such quantities and then we take the limit  $t \rightarrow \infty$ . Accordingly we have that

$$\partial_t \langle \mathbf{r}_i(t) \cdot \mathbf{r}_j(t) \rangle = \langle (\partial_t \mathbf{r}_i) \cdot \mathbf{r}_j \rangle + \langle \mathbf{r}_i(t) \cdot (\partial_t \mathbf{r}_j) \rangle \quad (17)$$

We start by computing  $\langle \partial_t \mathbf{r}_i(t) \cdot \mathbf{r}_j(t) \rangle$

$$\langle \partial_t \mathbf{r}_i(t) \cdot \mathbf{r}_j(t) \rangle = -\zeta_i \langle \mathbf{r}_i(t) \mathbf{r}_j(t) \rangle + \left\langle \mu \int_{-\frac{N}{2}}^{\frac{N}{2}} \frac{\sum_{n=0}^{\infty} \sum_{m=0}^{\infty} f_m \psi_m(s) \partial_s \psi_n(s) \mathbf{r}_n(t) \cdot \mathbf{r}_j(t)}{\sqrt{\sum_{m=0}^{\infty} \mathbf{r}_m \partial_s \psi_m(s) \cdot \sum_{n=0}^{\infty} \mathbf{r}_n \partial_s \psi_n(s)}} \psi_i(s) ds \right\rangle + \langle \boldsymbol{\eta}_i(t) \cdot \mathbf{r}_j(t) \rangle. \quad (18)$$

We approximate the last expression using a mean-field argument, that is, the relevant contributions to the noise average of the whole expression come from the noise average of the individual correlations; thus Eq. (18) can be written as:

$$\langle \partial_t \mathbf{r}_i(t) \cdot \mathbf{r}_j(t) \rangle = -\zeta_i \langle \mathbf{r}_i(t) \mathbf{r}_j(t) \rangle + \mu \int_{-\frac{N}{2}}^{\frac{N}{2}} \frac{\sum_{n=0}^{\infty} \sum_{m=0}^{\infty} f_m \psi_m(s) \partial_s \psi_n(s) \langle \mathbf{r}_n(t) \cdot \mathbf{r}_j(t) \rangle}{\sqrt{\sum_{m=0}^{\infty} \sum_{n=0}^{\infty} \partial_s \psi_n(s) \partial_s \psi_m(s) \langle \mathbf{r}_m \cdot \mathbf{r}_n \rangle}} \psi_i(s) ds + \langle \boldsymbol{\eta}_i(t) \cdot \mathbf{r}_j(t) \rangle \quad (19)$$

One can derive an equivalent expression for  $\langle \mathbf{r}_i(t) \cdot \partial_t \mathbf{r}_j(t) \rangle$  by simply interchanging  $i$  and  $j$  in Eq. (19). Following Eq. (17), summing  $\langle \partial_t \mathbf{r}_i(t) \cdot \mathbf{r}_j(t) \rangle$  (that is, Eq. (19)) and  $\langle \mathbf{r}_i(t) \cdot \partial_t \mathbf{r}_j(t) \rangle$  we obtain

$$\begin{aligned} \partial_t \langle \mathbf{r}_i(t) \cdot \mathbf{r}_j(t) \rangle &= -\zeta_i \langle \mathbf{r}_i(t) \mathbf{r}_j(t) \rangle + \mu \int_{-\frac{N}{2}}^{\frac{N}{2}} \frac{\sum_{n=0}^{\infty} \sum_{m=0}^{\infty} f_m \psi_m(s) \partial_s \psi_n(s) \langle \mathbf{r}_n(t) \cdot \mathbf{r}_j(t) \rangle}{\sqrt{\sum_{m=0}^{\infty} \sum_{n=0}^{\infty} \partial_s \psi_n(s) \partial_s \psi_m(s) \langle \mathbf{r}_m \cdot \mathbf{r}_n \rangle}} \psi_i(s) ds + \langle \boldsymbol{\eta}_i(t) \cdot \mathbf{r}_j(t) \rangle \\ &\quad - \zeta_j \langle \mathbf{r}_j(t) \mathbf{r}_i(t) \rangle + \mu \int_{-\frac{N}{2}}^{\frac{N}{2}} \frac{\sum_{n=0}^{\infty} \sum_{m=0}^{\infty} f_m \psi_m(s) \partial_s \psi_n(s) \langle \mathbf{r}_n(t) \cdot \mathbf{r}_i(t) \rangle}{\sqrt{\sum_{m=0}^{\infty} \sum_{n=0}^{\infty} \partial_s \psi_n(s) \partial_s \psi_m(s) \langle \mathbf{r}_m \cdot \mathbf{r}_n \rangle}} \psi_j(s) ds + \langle \boldsymbol{\eta}_j(t) \cdot \mathbf{r}_i(t) \rangle \end{aligned} \quad (20)$$

By putting to zero the lhs of Eq. (20) we can derive closed expressions for  $\langle \mathbf{r}_i(t) \cdot \mathbf{r}_j(t) \rangle^\infty$ . In order to simplify the notation we introduce

$$\langle \Theta(s) \rangle = \sum_{m=0}^{\infty} \sum_{n=0}^{\infty} \partial_s \psi_n(s) \partial_s \psi_m(s) \langle \mathbf{r}_m \cdot \mathbf{r}_n \rangle^\infty \quad (21)$$

By substituting Eqs. (21) into Eq. (20) and putting the lhs to zero we get

$$\begin{aligned} \langle \mathbf{r}_i \cdot \mathbf{r}_j \rangle^\infty &= \frac{\mu}{\Gamma_{ij}} \sum_m f_m \left[ \sum_{n \neq i} \langle \mathbf{r}_n \cdot \mathbf{r}_j \rangle^\infty \int_{-\frac{N}{2}}^{\frac{N}{2}} \frac{\psi_m(s) \partial_s \psi_n(s)}{\sqrt{\langle \Theta(s) \rangle}} \psi_i(s) ds + \sum_{n \neq j} \langle \mathbf{r}_n \cdot \mathbf{r}_i \rangle^\infty \int_{-\frac{N}{2}}^{\frac{N}{2}} \frac{\psi_m(s) \partial_s \psi_n(s)}{\sqrt{\langle \Theta(s) \rangle}} \psi_j(s) ds \right] + \\ &\quad + \frac{\langle \boldsymbol{\eta}_j \cdot \mathbf{r}_i \rangle^\infty + \langle \boldsymbol{\eta}_i \cdot \mathbf{r}_j \rangle^\infty}{\Gamma_{ij}} \end{aligned} \quad (22)$$

where

$$\Gamma_{ij} = \zeta_i + \zeta_j - \mu \sum_m f_m \int_{-\frac{N}{2}}^{\frac{N}{2}} \frac{\psi_m(s) \psi_i(s) \partial_s \psi_i(s) + \psi_m(s) \psi_j(s) \partial_s \psi_j(s)}{\sqrt{\langle \Theta(s) \rangle}} ds. \quad (23)$$

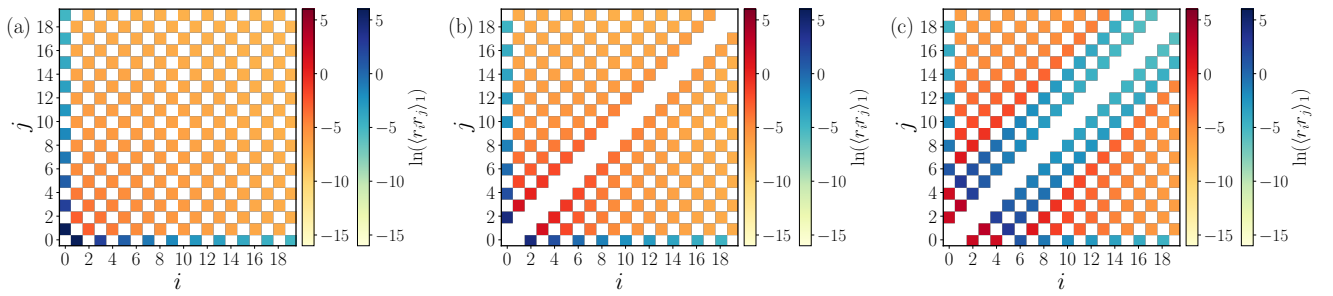


FIG. 2:  $\langle \mathbf{r}_i \cdot \mathbf{r}_j \rangle_1^\infty$  with  $l_p = 0.5$ ,  $N = 100$ , and  $f_m = 1$  and (a)  $m = 0$ , (b)  $m = 1$ , (c)  $m = 5$ . The color codes represents the logarithm of the magnitude of the correlations, using warm colors for positive magnitudes and cool colors for negative magnitudes.

### C. Small force expansion

In the following we expand the amplitudes of the modes about the value they attain at zero active force,  $f_i = 0, \forall i$ . Typically, when expanding, it is important to identify a small dimensionless number; here we should define the relevant Péclet number by multiplying the active force by the relevant length scale and dividing by the thermal energy. In particular, we need to ensure that the terms proportional to the active force are small for all values of the polymer length  $N$ ; hence, we expect a possible coupling between the magnitude of the active force and the length of the polymer for which the terms proportional to the active force are small. However, *a priori* it is not obvious to identify the relevant length scale. Therefore we proceed with the expansion by neglecting terms that quadratic or more in the active force. At the end of the expansion we will identify and discuss the relevant Péclet number. From Eq. (22) we have, at zeroth order,

$$\sum_m f_m \left[ \sum_{n \neq i} \langle \mathbf{r}_n \cdot \mathbf{r}_j \rangle_0^\infty \int_{-\frac{N}{2}}^{\frac{N}{2}} \frac{\psi_m(s) \partial_s \psi_n(s)}{\sqrt{\langle \Theta(s) \rangle_0}} \psi_i(s) ds + \sum_{n \neq j} \langle \mathbf{r}_n \cdot \mathbf{r}_i \rangle_0^\infty \int_{-\frac{N}{2}}^{\frac{N}{2}} \frac{\psi_m(s) \partial_s \psi_n(s)}{\sqrt{\langle \Theta(s) \rangle_0}} \psi_j(s) ds \right] \ll \frac{\langle \boldsymbol{\eta}_j \cdot \mathbf{r}_i \rangle_0^\infty + \langle \boldsymbol{\eta}_i \cdot \mathbf{r}_j \rangle_0^\infty}{\mu} \quad (24)$$

where the subscript 0 indicate that the averages are done at  $f_i = 0$ . In particular, in the absence of active force we have that

$$\langle \boldsymbol{\eta}_j \cdot \mathbf{r}_i \rangle_0^\infty = \langle \boldsymbol{\eta}_j \cdot \mathbf{r}_i^{(0)} \rangle_0^\infty = \lim_{t \rightarrow \infty} \int_0^t e^{-\frac{\Gamma_{ii}^{(0)}}{2}(t-\tau)} \langle \boldsymbol{\eta}_i(\tau) \cdot \boldsymbol{\eta}_j(t) \rangle d\tau = \delta_{ij} 2d\mu k_B T \quad (25)$$

where  $\mathbf{r}_i^{(0)}(t)$  is the zeroth-order solution obtained from Eq. (15) and  $d$  is the dimension of the space in which the polymer is embedded in. Hence we have

$$\langle \mathbf{r}_i \cdot \mathbf{r}_j \rangle_0^\infty = \lim_{t \rightarrow \infty} \int_0^t \int_0^t e^{-\frac{\Gamma_{ii}^{(0)}}{2}(t-\tau_1)} e^{-\frac{\Gamma_{jj}^{(0)}}{2}(t-\tau)} \delta_{ij} \langle \boldsymbol{\eta}_i(\tau_1) \cdot \boldsymbol{\eta}_j(\tau) \rangle d\tau d\tau_1 = \delta_{ij} d \frac{\mu k_B T}{\zeta_i} \quad (26)$$

Higher order corrections can then be computed similarly and are reported in Appendix A 1.

### D. Short persistence length

The calculations and the expressions can be further simplified if the persistence length is much shorter than the polymer length, that is,  $l_p \ll N\sigma$ . This case is not only convenient from the technical perspective, but it is also most relevant from the physical one since flexible polymers are, naturally, more affected by activity with respect to their rigid counterparts, especially from the perspective of the polymer conformations. In this regime, the relation  $\beta_n^2 = k_n^2 + 1/l_p^2 \gg N$  holds and, accordingly, the hyperbolic functions are of order unity only in the vicinity of the edges of the polymer. In such a regime, we can approximate  $k_n = \frac{\pi n}{N}$  and take  $\beta_n \rightarrow \infty$  and hence the eigenfunction can be approximated by their trigonometric contribution. In order to simplify the notation, it is more convenient

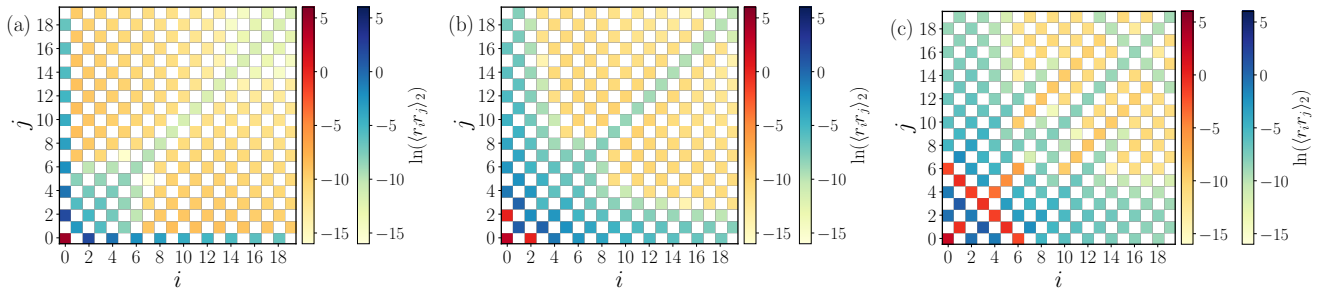


FIG. 3:  $\langle \mathbf{r}_i \cdot \mathbf{r}_j \rangle_2^\infty$  with  $l_p = 0.5$ ,  $N = 100$ , and  $f_m = 1$  and (a)  $m = 0$ , (b)  $m = 1$ , (c)  $m = 5$ . The color codes represents the logarithm of the magnitude of the correlations, using warm colors for positive magnitudes and cool colors for negative magnitudes.

to map the position along the backbone,  $s$ , on  $s \in [0 : N]$  rather than  $s \in [-N/2 : N/2]$ ; the boundary conditions (Eqs.(5), (6)) are then evaluated at  $s = 0, N$  and the eigenfunctions read:

$$\psi_0 = \sqrt{\frac{1}{N}} \quad (27a)$$

$$\psi(s)_n = \sqrt{\frac{2}{N}} \cos(k_n s) \quad (27b)$$

Further, we rewrite the eigenvalues as

$$\zeta_i = \mu k_i^2 (G k_i^2 + D) = \mu i^2 Q (\Lambda_p i^2 + 1), \quad \text{where} \quad Q = \frac{D \pi^2}{N^2}, \quad \Lambda_p = \frac{l_p^2 \pi^2}{N^2} \quad (28)$$

and we represent the external force as

$$f(s) = \sum_n f_n \cos(k_n s) \quad (29)$$

We notice that one can select a single mode in this representation, as will be done in Sec. III, (Eq. (36)); for example, selecting  $n = 1$  means  $f_1 = f^a$  and  $f_n = 0$  for  $n \neq 1$ . We will refer to this choice as a “single-mode” force (see Fig. 1a). By employing the simplified expressions introduced above, we can rewrite the correlation functions  $\langle \mathbf{r}_i \cdot \mathbf{r}_j \rangle_2^\infty$  at different orders. The details of the expansion are provided in Appendix A 2; here we just report the final expressions for a single-mode force of mode  $l$ :

$$\langle \mathbf{r}_i \cdot \mathbf{r}_j \rangle_0^\infty = \delta_{ij} d \frac{k_B T N^2}{\pi^2 D} \frac{1}{\bar{z}_i} \quad (30a)$$

$$\langle \mathbf{r}_i \cdot \mathbf{r}_j \rangle_1^\infty = -8\sqrt{2} \frac{b^2 N^2}{\pi^4 d^2} \frac{1}{l_p^2} \frac{(1 - \delta_{ij})}{\bar{z}_i + \bar{z}_j} \text{Pe}_l \left( \frac{\bar{\xi}_{ijl}^{(0)}}{\bar{z}_j} + \frac{\bar{\xi}_{jil}^{(0)}}{\bar{z}_i} \right) \quad (30b)$$

$$\begin{aligned} \langle \mathbf{r}_i \cdot \mathbf{r}_j \rangle_2^\infty = & \frac{64}{\pi^6} \frac{b^2 N^2}{l_p d^3} \frac{1}{\bar{z}_i + \bar{z}_j} \text{Pe}_l^2 \left[ \sum_{n \neq i} \frac{1 - \delta_{jn}}{\bar{z}_n + \bar{z}_j} \left( \frac{\bar{\xi}_{jnl}^{(0)}}{\bar{z}_n} + \frac{\bar{\xi}_{njl}^{(0)}}{\bar{z}_j} \right) \bar{\xi}_{inm}^{(0)} + \sum_{n \neq j} \frac{1 - \delta_{in}}{\bar{z}_n + \bar{z}_i} \left( \frac{\bar{\xi}_{inl}^{(0)}}{\bar{z}_n} + \frac{\bar{\xi}_{nil}^{(0)}}{\bar{z}_i} \right) \bar{\xi}_{jnm}^{(0)} \right] + \\ & - \frac{8b^2 N^2}{d \pi^6} \frac{1 - \delta_{ij}}{\bar{z}_i + \bar{z}_j} \text{Pe}_l \left[ \frac{\bar{\xi}_{ijr}^{(1)}}{\bar{z}_j} + \frac{\bar{\xi}_{jir}^{(1)}}{\bar{z}_i} \right] - \delta_{ij} \frac{8b^2 N^2}{\pi^6 d} \frac{1}{\bar{z}_i^2} \text{Pe}_l \bar{\xi}_{iir}^{(1)} \end{aligned} \quad (30c)$$

where

$$\bar{z}_i = i^2 (1 + \Lambda_p i^2) \quad (31)$$

are the normalized eigenvalues and  $\xi^{(0)}, \xi^{(1)}$  are some trigonometric integrals defined in Appendix A 1. It is interesting to note that by introducing the Péclet number

$$\text{Pe}_m = \frac{f_m b \sqrt{N}}{k_B T} \quad (32)$$

the expressions in Eqs. (30) share the same scaling with  $N$ . Accordingly, Eq. (32) identifies the relevant Péclet number for which the terms proportional to the active force are smaller than the passive one irrespectively of the polymer length,  $N$ . It is interesting to note that such a Péclet number has been also empirically derived in Ref. [34]. For later use, we report the values of  $\langle \mathbf{r}_n \cdot \mathbf{r}_m \rangle_1^\infty$  (Fig.2) and  $\langle \mathbf{r}_n \cdot \mathbf{r}_m \rangle_2^\infty$  (Fig.3)

### III. NUMERICAL MODEL AND SIMULATION DETAILS

We model active polymer chains as semi-flexible Gaussian beads-spring linear chains consisting of  $N$  monomers, suspended in a 3D bulk fluid. Since we consider Gaussian polymers, non-neighbouring monomers do not interact with each other. To guarantee chain connectivity, neighbouring monomers interact via the combination of the truncated and shifted Lennard-Jones potential (also known as WCA) and the Finitely Extensible Nonlinear Elastic (FENE) potential. The truncated and shifted Lennard-Jones (LJ) potential reads

$$V_{\text{LJ}}(r) = \begin{cases} 4\epsilon \left[ \left(\frac{\sigma}{r}\right)^{12} - \left(\frac{\sigma}{r}\right)^6 + \frac{1}{4} \right] & \text{for } r < 2^{1/6}\sigma \\ 0 & \text{for } r \geq 2^{1/6}\sigma \end{cases} \quad (33)$$

where  $\sigma = 1$  is the diameter of the monomer and is taken as the unit of length,  $\epsilon = 10 k_B T$  with  $k_B T = 1$  the energy scale and  $r = |\vec{r}_i - \vec{r}_j|$  is the Euclidean distance between the monomers  $i$  and  $j$  positioned at  $\vec{r}_i$  and  $\vec{r}_j$ , respectively. The Finitely Extensible Nonlinear Elastic (FENE) potential reads

$$V_{\text{FENE}}(r) = -\frac{K r_0^2}{2} \ln \left[ 1 - \left( \frac{r}{r_0} \right)^2 \right] \quad (34)$$

with  $K = 30 \epsilon / \sigma^2 = 300 k_B T / \sigma^2$  and  $r_0 = 1.5\sigma$ . The combination of FENE and WCA provides a typical bond length  $b \simeq 0.97\sigma$  and, with the chosen parameters, the bond length remains fixed even at the highest values of the active force considered in this work. The polymer rigidity is introduced with the bending potential:

$$U_b(\theta) = \kappa(1 + \cos \theta), \quad (35)$$

where  $\theta$  is the angle formed by three consecutive beads along the backbone and  $\kappa = 3k_B T$  is the bending energy; this results in a persistence length  $l_p/L = \kappa/(k_B T N) = 0.0075$ , for  $N = 400$ .

Activity is introduced as a tangential self-propulsion[32], where an active monomer  $i$  at position  $\vec{r}_i$  is subject to an active force  $\vec{f}_i^a$  parallel to the normalized tangent vector  $\hat{t}_i = (\vec{r}_{i+1} - \vec{r}_{i-1})/|\vec{r}_{i+1} - \vec{r}_{i-1}|$ ; the end monomers are always passive. In this work, we modulate the force on each bead via a sinusoidal function of the bead index along the polymer, that can be tuned by a parameter  $m$ , assuming only integer values ( $m \in \mathbb{N}$ ). Overall, the active force on bead  $2 \leq i \leq N - 1$  reads

$$\vec{f}_i^a(m) = f^a \cos\left(\frac{\pi m}{N} i\right) \hat{t}_i. \quad (36)$$

where  $f^a$  is the strength of the activity. Notice that with this prescription, the magnitude of the active force is not constant along the chain for  $m \neq 0$ .

We simulate polymers in bulk conditions via periodic boundary conditions, employing the open source code LAMMPS[38], with in-house modifications to implement the tangential activity Eq. (36). Langevin Dynamics simulations are performed, disregarding hydrodynamic interactions. The equations of motion are integrated using the velocity Verlet algorithm, with an elementary time step  $\Delta t = 10^{-3}$ . Units of mass, length, and energy are set to  $\bar{m} = 1$ ,  $\sigma = 1$ , and  $k_B T = 1$ , respectively. The unit of time is  $\tau = \sqrt{\bar{m}\sigma^2/k_B T} = 1$ . The overdamped regime is ensured by setting the friction coefficient  $\gamma = 20 k_B T \tau / \sigma^2$  for  $\text{Pe} > 1$  [39]; otherwise, we set  $\gamma = 1 k_B T \tau / \sigma^2$ . We perform simulations varying the activity  $f^a = 0.001, 0.01, 1, 10 k_B T / \sigma$ , the polymer length  $N = 200, 400$  and the force mode  $m = 0, 1, 2, 3, 4, 5, 6, 7, 8, 11, 14, 20, 40, 100$ ; we collect data over  $M = 25$  independent trajectories for each set of parameters. After reaching a steady state, production runs are performed for  $\simeq 2 \cdot 10^8$  time steps ( $2 \cdot 10^5 \tau$ ) and the polymer conformations are sampled at a rate of  $10^6$  time steps ( $2 \cdot 10^3 \tau$ ).

### IV. RESULTS

Before carrying on a direct comparison between theory and simulation results, we briefly show and discuss the phenomenology that emerges from simulations. Figures 4, 5, as well as Fig. 1b), report snapshot of polymer conformations from numerical simulations of fixed degree of polymerization  $N = 200$  beads and  $\text{Pe}_m = 141.42$ . We remark

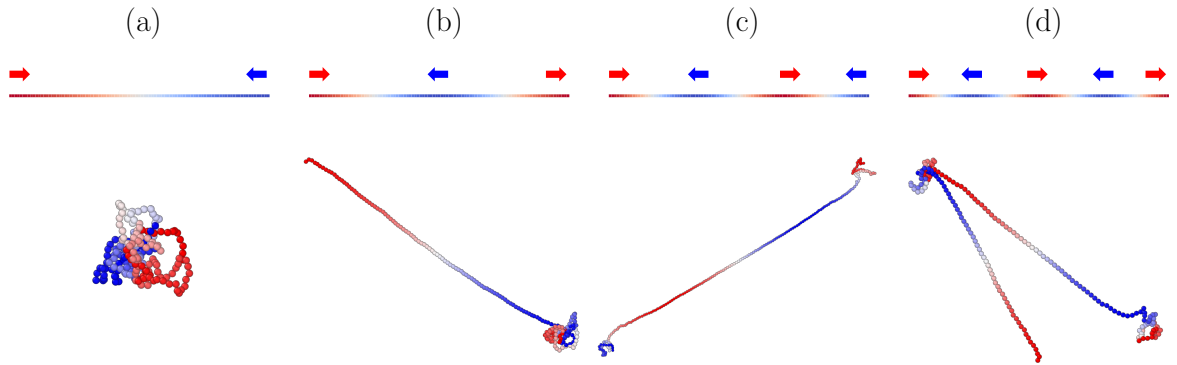


FIG. 4: Snapshots of active polymers,  $N = 200$ ,  $Pe = 10$  and different values of the active force mode  $m$ . The chosen color map highlights both the sign and magnitude of the active force, shades of red being positive, shades of blue being negative and white being zero; arrows indicate the overall direction of the force in the section of the chain close to the arrow. (a)  $m = 1$ , (b)  $m = 2$ , (c)  $m = 3$ , (d)  $m = 4$ .

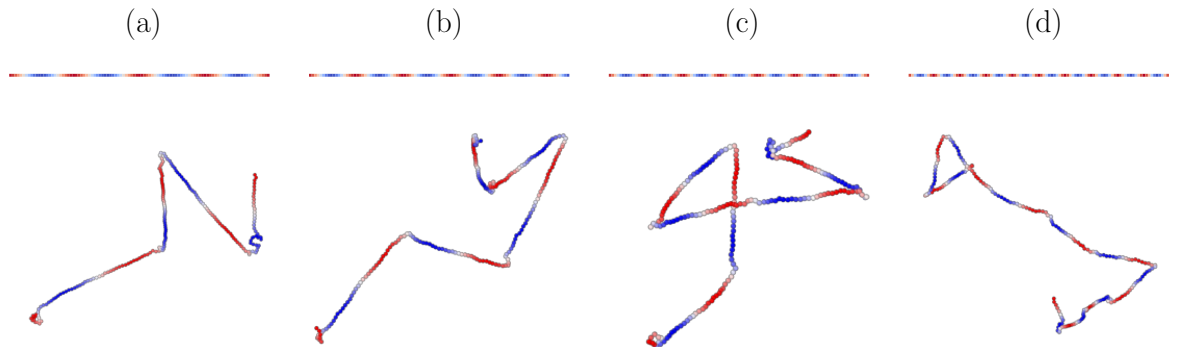


FIG. 5: More snapshots of active polymers,  $N = 200$ ,  $Pe = 10$  and different values of the active force mode  $m$ . Color map as in Fig. 4. (a)  $m = 8$ , (b)  $m = 11$ , (c)  $m = 14$ , (d)  $m = 20$ .

that our theoretical approach is valid at sufficiently low activity; nevertheless, the phenomenology is more evident at high values of  $Pe_m$  and, for such reason, we use this case for showcasing the effect of the active force modulation. The snapshots are color-coded to highlight the force modulation: the color code highlights both the sign and magnitude of the active force, shades of red being positive, shades of blue being negative and white being zero. The force modulation is then visible on the conformations and is explicitly reported on the colorbars above the snapshots. At low values of  $m$  we add arrows above the colorbars to indicate the direction of the active force (see Fig. 4); for large values of  $m$ , this representation becomes impractical and, thus, arrows are omitted in Fig. 5.

First, we notice that, in the case  $m = 1$  (Fig. 4a), the polymer conformation is considerably more compact than in all the other cases and reminds of the globule-like conformations observed in a tangentially active polymer [32], which is recovered in this framework as the case  $m = 0$ . However, for  $m > 1$  the conformations appear much more elongated, with visibly stretched and visibly compact regions, especially at low values of  $m$ . The snapshots suggests that the appearance of these regions depends on the alternation of the direction of propulsion, that is, on the alternation of positive and negative propulsion sections. If, proceeding along the chain, a negative section comes after a positive one,

the corresponding polymer region is collapsed, as the active forces (showed with arrows in Fig. 4) point towards each other, causing the filament to buckle. On the contrary, if a positive section follows a negative one the corresponding polymer region is stretched as the active forces point away from each other. The higher the value of  $m$ , the more stretched sections the polymer can develop; since the polymer is Gaussian, the stretched regions are independent from each other and can arrange freely in space (see Fig. 1b and 5).

### A. Gyration Radius

We now turn to the typical quantities that characterize the conformations of the polymers. The gyration tensor is defined as:

$$\langle S_{ij}(t) \rangle = \left\langle \frac{1}{N} \int_0^N (r_i(s, t) - r_{0,i}(t))(r_j(s, t) - r_{0,j}(t)) ds \right\rangle \quad (37)$$

where  $\mathbf{r}_0(t)$  is the location of the center of mass. In the cosines representation  $S$  reads:

$$\langle S_{ij}(t) \rangle = \left\langle \frac{2}{N^2} \int \sum_{n,m} r_{n,i}(t) r_{m,j}(t) \cos(k_n s) \cos(k_m s) - \sum_n [r_{0,i}(t) r_{n,j}(t) + r_{0,j}(t) r_{n,i}(t)] \cos(k_n s) + r_{0,i} r_{0,j} ds \right\rangle \quad (38)$$

that finally reads:

$$\langle S_{ij}(t) \rangle = \frac{1}{N} \left[ \sum_{n \neq 0} \langle r_{n,i}(t) r_{n,j}(t) \rangle - \langle r_{0,i} r_{0,j} \rangle \right] = \frac{1}{N} \left[ \sum_{n \neq 0} \langle r_{n,i}(t) r_{n,j}(t) \rangle \right] \quad (39)$$

The gyration tensor is symmetric and hence it can be diagonalized; the gyration radius is the trace of  $S$ ,  $\mathcal{R}_G^2 = \text{Tr}S$ . At zeroth order we have

$$\mathcal{R}_{G,0} = \frac{1}{6} \frac{dk_B T N}{D \pi^2} \left( 3\Lambda_p - 3\pi \Lambda_p \coth \left( \frac{\pi}{\Lambda_p} \right) + \pi^2 \right) = \frac{2l_p b^2 N}{6\pi^2} \left( 3\Lambda_p - 3\pi \Lambda_p \coth \left( \frac{\pi}{\Lambda_p} \right) + \pi^2 \right) \quad (40)$$

where we have used Eqs. (4); note that for  $\Lambda_p \rightarrow 0$  (that is, for  $N \rightarrow \infty$ ) we retrieve  $\mathcal{R}_{G,0} \simeq \frac{1}{6} b^2 N$ , that is, the zeroth order of our expansion correctly yields the equilibrium value at  $f_m = 0$ .

At first order, the diagonal corrections are null,  $\langle \mathbf{r}_n \cdot \mathbf{r}_n \rangle_1^\infty = 0$  (see Eq. (A11)), and hence  $\mathcal{R}_{G,1} = 0$ . At second order, the correction to  $\mathcal{R}_G^2$  depends on the extensibility of the polymer. As we discuss in Appendix A 4, in order to ensure that the polymer length does not vary upon applying the active force, the stretching coefficient  $D$  has to be adjusted (see Eq. (A40)). Accordingly, by substituting Eq. (A40) into Eq. (40) we get<sup>1</sup>:

$$\mathcal{R}_{G,D} = -\frac{\bar{D}_2}{D} \mathcal{R}_{G,0} = -\frac{1}{6} \frac{dk_B T N}{D} \frac{\bar{D}_2}{D} \quad (41)$$

where in the last step we took the limit  $\Lambda_p \ll 1$ . Accordingly, at second order, we get

$$\mathcal{R}_{G,2} = \frac{1}{2N} \sum_i \langle \mathbf{r}_n \cdot \mathbf{r}_n \rangle_2^\infty - \frac{1}{6} \frac{dk_B T N}{D} \frac{\bar{D}_2}{D} \quad (42)$$

Figure 6 reports the comparison between the numerical results (Fig. 6a) and the theoretical results (Fig. 6b,c). Fig. 6a reports the ratio of the squared gyration radius  $\mathcal{R}_G^2$  over its equilibrium counterpart  $(\mathcal{R}_G^0)^2$ , at fixed active force ( $f^a = 0.01, 10 k_B T / \sigma$ ) for polymers of length  $N = 200, 400$  beads, so that the value of  $\text{Pe}_m$  varies for the two different polymers. In both the upper and lower sub-panels, we find a phenomenology consistent with our previous observations: for  $m \leq 1$  the polymer shrinks ( $\mathcal{R}_G^2 / (\mathcal{R}_G^0)^2 < 1$ ) and for  $m > 1$  the polymer swells ( $\mathcal{R}_G^2 / (\mathcal{R}_G^0)^2 > 1$ ). Notice that, for large values of  $m$   $\mathcal{R}_G^2 / (\mathcal{R}_G^0)^2 \simeq 1$ : in this limit the polymer becomes a succession of short stretched regions, independent from each other, that can arrange freely in space, producing a coil-like conformation.

<sup>1</sup> In principle the same rationale applies also at first order. However,  $D_1 = 0$  and there is no contribution from the corrections to the stretching coefficient at first order.

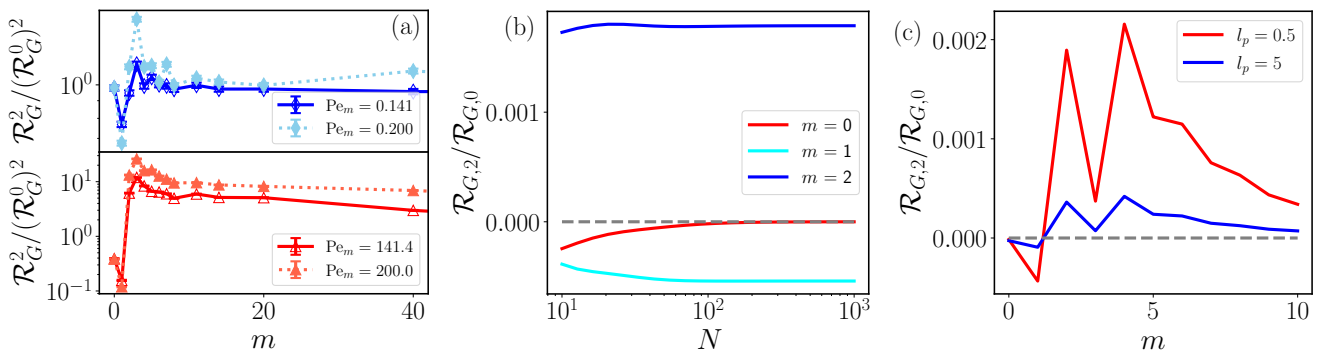


FIG. 6: (a) Ratio of the gyration radius, over the equilibrium value  $\mathcal{R}_G^2/(\mathcal{R}_G^0)^2$  as a function of the mode  $m$  and different values of  $\text{Pe}_m$  (with full lines  $N = 200$  and dotted lines  $N = 400$ ) from numerical simulations. (b)  $\mathcal{R}_{G,2}$  (Eq. (42)), normalized by the equilibrium gyration radius,  $\mathcal{R}_{G,0}$ , as a function of  $N$  for and  $l_p = 0.5$  and various values of the force mode  $m$ ; (c)  $\mathcal{R}_{G,2}/\mathcal{R}_{G,0}$  as function of the mode  $m$ , for  $N = 100$  and different values of  $l_p$ .

In order to compare numerical and theoretical results, one has to evaluate the corrections to the zeroth order, that is Eq. (42). We show the relative importance of this second-order correction, with respect to the zero-order one, for  $\text{Pe}_m = 1$  in Fig. 6b,c as a function of  $N$  and  $m$ , respectively. Interestingly, at fixed  $\text{Pe}_m$ , the correction becomes constant or negligible with increasing  $N$ ; in simulations, as we do not change the active force to keep  $\text{Pe}_l$  fixed, we see the effects of the activity are more pronounced for larger polymers, in agreement with the theoretical trends. Further, notice that the corrections for  $m = 0$  are negative, that is, the gyration radius decreases when  $f^a \neq 0$ , in qualitative agreement with previous numerical results [32]. For  $m = 1$  the correction remains negative, meaning that the model predicts a shrinking of  $\mathcal{R}_G$ , as reported in simulations. Instead, with increasing  $m$ , the correction becomes positive, that is, the gyration radius increases as observed, again, in simulations. Furthermore, at large values of  $m$ , the correction becomes negligible, again in qualitative agreement with simulations. We highlight that the theory predicts a larger increase of  $\mathcal{R}_G$  for  $m = 2, 4$ , whereas simulations data report a maximum of  $\mathcal{R}_G$  for  $m = 3$ ; this discrepancy could be caused by the use, in the numerical model, of anharmonic springs (FENE) or by the impossibility to include the correct boundary conditions in the theoretical model.

## B. End-to-end vector

The second and last conformational quantities that we consider is the square end-to-end distance at steady state:

$$\begin{aligned}
 \mathcal{R}_E^2 &= \langle (\mathbf{r}_n - \mathbf{r}_0) \cdot (\mathbf{r}_n - \mathbf{r}_0) \rangle = \int_0^N ds \int_0^N dw \langle r'(s) \cdot r'(w) \rangle^\infty \\
 &= \frac{2}{N} \int_0^N ds \int_0^N dw \sum_{n=0}^{\infty} \langle \mathbf{r}_n k_n \sin(k_n s) \cdot \sum_{m=0}^{\infty} \mathbf{r}_m k_m \sin(k_m w) \rangle^\infty \\
 &= \frac{8}{N} \sum_{n=\text{odd}} \sum_{m=\text{odd}} \langle \mathbf{r}_n \cdot \mathbf{r}_m \rangle^\infty
 \end{aligned} \tag{43}$$

At zeroth order we have:

$$\begin{aligned}
 \mathcal{R}_{E,0} &= \frac{8}{N} \sum_{n=\text{odd}} \sum_{m=\text{odd}} \langle \mathbf{r}_n \cdot \mathbf{r}_m \rangle_0^\infty = \frac{8}{N} \sum_{n=\text{odd}} \frac{dk_B T}{n^2 Q (1 + \Lambda_p n^2)} = d \frac{\pi}{N} \frac{k_B T}{Q} \left( \pi - 2\sqrt{\Lambda_p} \tanh \left( \frac{\pi}{2\sqrt{\Lambda_p}} \right) \right) \\
 &= \frac{dN k_B T}{\pi D} \left( \pi - 2\Lambda_p \tanh \left( \frac{\pi}{2\Lambda_p} \right) \right)
 \end{aligned} \tag{44}$$

where we use the definitions of  $Q$  and  $\Lambda_p$ , Eqs. (28); note that for  $\Lambda_p \rightarrow 0$  and  $d = 3$  we retrieve the Rouse scaling  $\mathcal{R}_{E,0} \simeq b^2 N$  and the usual relation  $\mathcal{R}_{E,0} = 6\mathcal{R}_{G,0}$ .

We highlight that the first-order contribution depends on the parity of the active force. For active forces composed solely of the *even* modes, from Eq. (A27) we have  $\mathcal{R}_{E,1} = 0$ . In contrast, for active forces that accounts also for *odd*

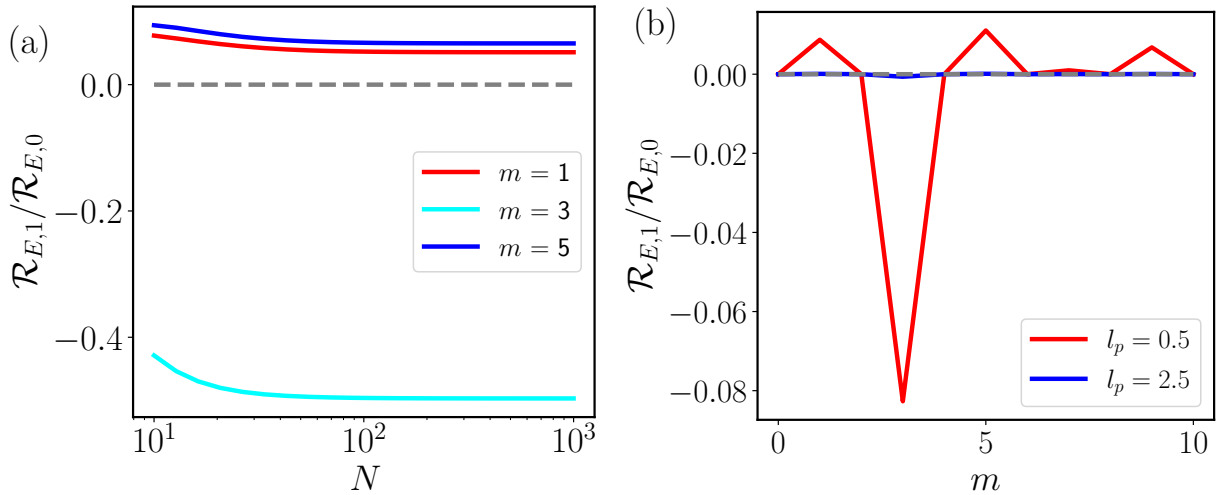


FIG. 7:  $\mathcal{R}_{E,1}$  (Eq. (45)), normalized by the equilibrium end-to-end distance,  $\mathcal{R}_{E,0}$ , for a single-mode force with  $\text{Pe}_l = 1$  (a)  $\mathcal{R}_{E,1}/\mathcal{R}_{E,0}$  as function of  $N$  for a single-mode force with  $l_p = 0.5$  and different values of  $m$ ; (b)  $\mathcal{R}_{E,1}/\mathcal{R}_{E,0}$  as function of  $m$  for a single-mode force with  $N = 100$  and different values of  $l_p$ .

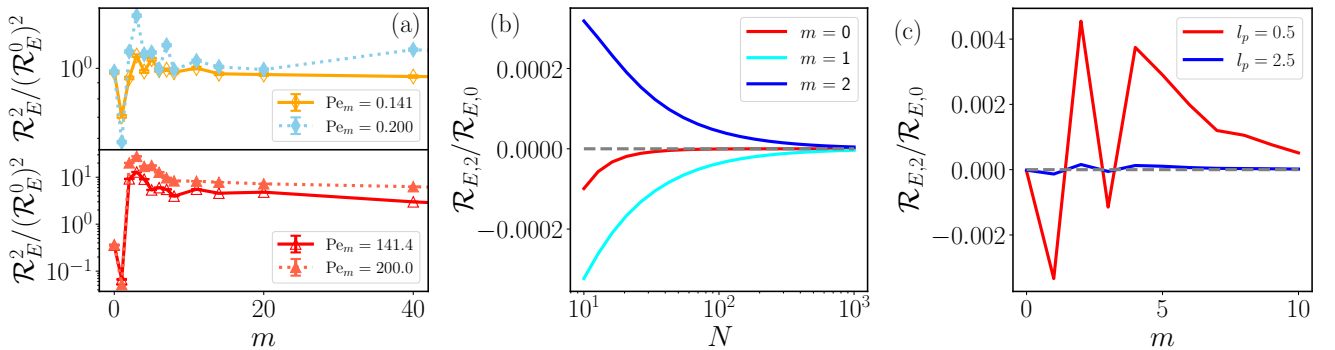


FIG. 8: (a) Ratio of the end-to-end square distance, over the equilibrium value  $\mathcal{R}_E^2/(\mathcal{R}_E^0)^2$  as a function of the mode  $m$  and different values of  $\text{Pe}_m$  (with full lines  $N = 200$  and dotted lines  $N = 400$ ) from numerical simulations. (b)  $\mathcal{R}_{E,2}$  (Eq. (46)), normalized by the equilibrium end-to-end distance,  $\mathcal{R}_{E,0}$ , as a function of  $N$  for and  $l_p = 0.5$  and various values of the force mode  $m$ ; (c)  $\mathcal{R}_{E,2}/\mathcal{R}_{E,0}$  as function of the mode  $m$ , for  $N = 100$  and different values of  $l_p$ .

modes we have

$$\mathcal{R}_{E,1} = \frac{8}{N} \sum_{n=\text{odd}} \sum_{m=\text{odd}} \langle \mathbf{r}_n \cdot \mathbf{r}_m \rangle_1^\infty \quad (45)$$

We remark that, as shown in Fig.2b, in the case of odd modes of the active force  $\langle \mathbf{r}_i \cdot \mathbf{r}_j \rangle_1^\infty \neq 0$  even when both  $i$ , and  $j$  are odds. In particular, the sign of  $\mathcal{R}_{E,1}$  changes upon flipping the sign of  $f_m$ , with  $m = \text{odd}$ , in Eq. (29). Surprisingly,  $\mathcal{R}_{E,1} < 0$  for  $m = 3$ , whereas  $\mathcal{R}_{E,1} > 0$  for  $m = 1$  and  $m \geq 5$ .

For active forces that are composed of solely *even* modes the leading corrections are quadratic in the magnitude of the force. Indeed, for  $m = \text{even}$ , at second order, using Eq. (42) we get

$$\mathcal{R}_{E,2} = \frac{8}{N} \sum_{n=\text{odd}} \sum_{m=\text{odd}} \langle \mathbf{r}_n \cdot \mathbf{r}_m \rangle_2^\infty - \frac{\overline{D}_2}{\overline{D}_0} \mathcal{R}_{E,0} \quad (46)$$

We plot our results in Fig. 8. Again, we first start from numerical results, plotting the ratio  $\mathcal{R}_E^2/(\mathcal{R}_E^0)^2$  as a function of  $m$ . In both upper and lower sub-panels of Fig. 8, data is consistent with the previous observations and with the results of Sec. IV A. In Fig. 8b,c, we plot the relative importance of the second-order correction with respect to the zeroth-order one at fixed  $\text{Pe}_m = 1$ . We remark that these corrections are present for all modes, but they are the

leading order correction for the even modes. We observe the same trends, reported for second order corrections of  $\mathcal{R}_G$ :  $\mathcal{R}_{E,2}$  becomes negligible with increasing  $N$  and  $m$  and oscillates at small values of  $m$ , being in particular negative for  $m = 0$  and  $m = 1$ . However, considering the first order corrections, the theory would predict an overall increase of  $\mathcal{R}_E$  for  $m = 1$  and an overall decrease for  $m = 3$ , in contrast to simulation results. This can be possibly due to the fact that we cannot perform simulation at arbitrary small values of  $Pe_m$  and hence higher order corrections can play a role. However, more in general, Figs. 6 and 8 show that the sign of both  $\mathcal{R}_{G,2}$  and  $\mathcal{R}_{E,2}$  changes when crossing a threshold value,  $m^* = 4$  in the analytical model  $m^* = 2$  in simulations. For  $m \geq m^*$  the chain swells, while the opposite holds for  $m < m^*$ .

### C. Harmonic interactions

The shrinking of gyration radius of active polymers upon increasing the active force, in principle, may be regarded as the outcome of an effective attraction among the monomers induced by the activity. Accordingly, in order to check if the behavior of active polymers can be mapped into that of passive polymers in bad solvents (hence experiencing an effective attraction among monomers) we briefly study the case in which there is a net attractive force among the monomers.

This amounts to adding an additional contribution

$$F_i = -\gamma \sum_j \mathbf{r}_j - \mathbf{r}_i = -\gamma N \mathbf{r}_{CM} + \gamma N \mathbf{r}_i \quad (47)$$

where  $\mathbf{r}_{CM} = \sum_j \mathbf{r}_j / N$  is the position of the center of mass of the polymer. Accordingly, in the continuum limit, the equation of motion for the position of each monomer read:

$$\dot{\mathbf{r}}(s, t) = \mu D \partial_s^2 \mathbf{r}(s, t) + \mu \gamma N \mathbf{r}(s, t) - \mu \gamma N \mathbf{r}_{CM}(t) + \eta(s, t) \quad (48)$$

Expanding for small values of  $\gamma$  we obtain, at  $\mathcal{O}(0)$ ,  $\langle \mathbf{r}_i \mathbf{r}_j^* \rangle_0 = \frac{k_B T}{i^2} \delta_{ij}$ , while, at  $\mathcal{O}(1)$

$$\langle \mathbf{r}_i \mathbf{r}_j^* \rangle_1 = -\frac{1}{D(i^2 + j^2)} [2\gamma N \langle \mathbf{r}_i \mathbf{r}_j^* \rangle_0 - \gamma N (\langle \mathbf{r}_{CM} \mathbf{r}_j^* \rangle_0 + \langle \mathbf{r}_i \mathbf{r}_{CM}^* \rangle_0)] \quad (49)$$

We remark that for  $i = j$  Eq.(49) reduces to

$$\langle \mathbf{r}_i \mathbf{r}_i^* \rangle_1 = -\frac{1}{2D i^2} [2\gamma N \langle \mathbf{r}_i \mathbf{r}_i^* \rangle_0 - 2\gamma N \langle \mathbf{r}_{CM} \mathbf{r}_i^* \rangle_0] \quad (50)$$

that for  $i \neq 0$  is non vanishing. Moreover, the sign of  $\gamma$  is controlling the sign of  $\langle \mathbf{r}_i \mathbf{r}_j^* \rangle_1$ : for  $\gamma > 0$  (i.e. attractive forces) we have a reduction of the gyration radius (i.e.  $\langle \mathbf{r}_i \mathbf{r}_j^* \rangle_1 < 0$ ) whereas the opposite holds for repulsive forces ( $\gamma < 0$ ). This pinpoints a crucial difference between the collapse due to *non-conservative* or *conservative* forces. Indeed, in a series of experiments where the strength of the force can be tuned, in the first case the gyration radius will have a quadratic dependence on the strength, whereas in the second case a linear dependence.

## V. CONCLUSIONS

In this work, we investigated how spatially modulated activity alters the conformational properties of semiflexible polymers, combining a systematic expansion at small active driving with numerical simulations. Our analysis reveals that active forces can profoundly reshape polymer conformations in ways that depend sensitively on both chain length and the spatial structure of the applied forcing. The perturbative expansion developed here provides analytical access to the regime of weak activity, but it cannot capture the scaling behavior characteristic of strongly driven polymers. Within its range of validity, however, the expansion highlights that longer chains exhibit a markedly enhanced sensitivity to activity, which effectively amplifies the influence of even modest forces.

Our analysis shows that, for the two lowest modes ( $m = 0, 1$ ) both theory and simulations yield a reduction of the end-to-end distance within the weak-force regime. For higher modes, the polymer instead develops alternating stretched and compressed regions, reflecting the imposed spatial modulation of propulsion. Moreover, our model predicts that activity affects different measures of polymer size in distinct ways. Corrections to the end-to-end distance are generally larger in magnitude than those to the gyration radius, owing to the disparate modal contributions that enter each quantity. As a consequence, active polymers may simultaneously display a reduced gyration radius and an

increased end-to-end distance, suggesting conformations that are globally compact yet with highly extended terminal segments.

The theoretical predictions also indicate a transition between shrinking and swelling behaviors as the force mode number increases, with a threshold value  $m^*$  separating these regimes. Although the precise value of  $m^*$  differs between theory and simulation—an effect attributable to model idealizations—both approaches consistently show that high-mode forcing produces globally swollen conformations composed of many locally stretched segments.

Finally, the parity properties of the mode structure imply that, at leading order in Péclet, activity does not modify the gyration radius for ring polymers, since only even modes contribute. This is clearly not true when higher order correction are accounted for, as it has been observed in numerical simulations [40–42]. This remarkable difference between linear and ring polymers highlights how topology and symmetry can strongly constrain the response of active filaments.

Overall, our findings demonstrate that even weak, spatially structured activity can induce rich and nontrivial conformational behavior in semiflexible polymers. These results pave the way for future studies of more complex force profiles, stronger driving, and topologically constrained architectures, where active forces may generate new forms of self-organization and mechanical response.

## VI. DATA AVAILABILITY

The data are publicly available at <https://doi.org/10.5281/zenodo.17953054>

- 
- [1] M. C. Marchetti, J.-F. Joanny, S. Ramaswamy, T. B. Liverpool, J. Prost, M. Rao, and R. A. Simha, *Reviews of Modern Physics* **85**, 1143 (2013).
  - [2] M. E. Cates and J. Tailleur, *Annu. Rev. Cond. Matt. Phys.* **6**, 219 (2015).
  - [3] E. Tjhung, C. Nardini, and M. E. Cates, *Proceedings of the National Academy of Sciences* **115**, E1174 (2018).
  - [4] V. Narayan, S. Ramaswamy, and N. Menon, *Science* **317**, 105 (2007).
  - [5] H. H. Wensink, J. Dunkel, S. Heidenreich, K. Drescher, R. E. Goldstein, H. Löwen, and J. M. Yeomans, *Proceedings of the National Academy of Sciences* **109**, 14308 (2012).
  - [6] D. Needleman and Z. Dogic, *Nature Reviews Materials* **2**, 17048 (2017).
  - [7] T. Vicsek, A. Czirók, E. Ben-Jacob, I. Cohen, and O. Shochet, *Physical Review Letters* **75**, 1226 (1995).
  - [8] J. Howard, *Mechanics of Motor Proteins and the Cytoskeleton* (Sinauer Associates, Sunderland, MA, 2001).
  - [9] B. Alberts, D. Bray, K. Hopkin, A. D. Johnson, J. Lewis, M. Raff, K. Roberts, and P. Walter, *Essential cell biology* (Garland Science, 2015).
  - [10] A. Zidovska, D. A. Weitz, and T. J. Mitchison, *Proceedings of the National Academy of Sciences* **110**, 15555 (2013).
  - [11] I. Eshghi, A. Zidovska, and A. Y. Grosberg, *Physical Review Letters* **131**, 048401 (2023).
  - [12] A. Mahajan, W. Yan, A. Zidovska, D. Saintillan, and M. J. Shelley, *Physical Review X* **12**, 041033 (2022).
  - [13] A. Goychuk, D. Kannan, A. K. Chakraborty, and M. Kardar, *Proceedings of the National Academy of Sciences* **120**, e2221726120 (2023).
  - [14] L. Remini, M. Segers, J. Palmeri, J.-C. Walter, A. Parmeggiani, and E. Carlon, *Physical Review E* **109**, 024408 (2024).
  - [15] G. J. Narlikar, R. Sundaramoorthy, and T. Owen-Hughes, *Cell* **154**, 490 (2013).
  - [16] E. Lauga and T. R. Powers, *Reports on Progress in Physics* **72**, 096601 (2009).
  - [17] M. K. Faluwiki, J. Cammann, M. G. Mazza, and L. Goehring, *Physical Review Letters* **131**, 158303 (2023).
  - [18] M. Kurjahn, L. Abbaspour, F. Papenfuß, P. Bittihn, R. Golestanian, B. Mahault, and S. Karpitschka, *Nature Communications* **15**, 9122 (2024).
  - [19] J. Rosko, R. N. Poon, K. Cremin, E. Locatelli, M. Coates, S. J. Duxbury, K. Randall, K. Croft, C. Valeriani, M. Polin, et al., *Elife* **13**, RP100768 (2025).
  - [20] A. Deblais, A. C. Maggs, D. Bonn, and S. Woutersen, *Phys. Rev. Lett.* **124**, 208006 (2020).
  - [21] A. Deblais, K. Prathyusha, R. Sinaasappel, H. Tuazon, I. Tiwari, V. P. Patil, and M. S. Bhamla, *Soft Matter* **19**, 7057 (2023).
  - [22] R. Sinaasappel, M. Fazelzadeh, T. Hooijschuur, Q. Di, S. Jabbari-Farouji, and A. Deblais, *Physical Review Letters* **134**, 128303 (2025).
  - [23] R. Dreyfus, J. Baudry, M. L. Roper, M. Fermigier, H. A. Stone, and J. Bibette, *Nature* **437**, 862 (2005).
  - [24] R. Chelakkot, A. Gopinath, L. Mahadevan, and M. F. Hagan, *Journal of The Royal Society Interface* **11**, 20130884 (2014).
  - [25] H. R. Vutukuri, B. Bet, R. Van Roij, M. Dijkstra, and W. T. Huck, *Scientific reports* **7**, 16758 (2017).
  - [26] D. Nishiguchi, J. Iwasawa, H.-R. Jiang, and M. Sano, *New Journal of Physics* **20**, 015002 (2018), ISSN 1367-2630.
  - [27] Q. Martinet, Y. Li, A. Aubret, E. Hannezo, and J. Palacci, *Physical Review X* **15**, 041017 (2025).
  - [28] M. Kumar, A. Murali, A. G. Subramaniam, R. Singh, and S. Thutupalli, *Nature Communications* **15**, 4903 (2024).
  - [29] A. G. Subramaniam, M. Kumar, S. Thutupalli, and R. Singh, *New Journal of Physics* **26**, 083009 (2024).

- [30] Y. Ozkan-Aydin, D. I. Goldman, and M. S. Bhamla, Proceedings of the National Academy of Sciences **118**, e2010542118 (2021).
- [31] K. Becker, C. Teeple, N. Charles, Y. Jung, D. Baum, J. C. Weaver, L. Mahadevan, and R. Wood, Proceedings of the National Academy of Sciences **119**, e2209819119 (2022).
- [32] V. Bianco, E. Locatelli, and P. Magaretti, Phys. Rev. Lett. **121**, 217802 (2018).
- [33] R. E. Isele-Holder, J. Elgeti, and G. Gompper, Soft Matter **11**, 7181 (2015), ISSN 1744-683X, URL <http://xlink.rsc.org/?DOI=C5SM01683E>.
- [34] P. Magaretti, E. Locatelli, and C. Valeriani, Molecular Physics p. e2384462 (2024).
- [35] S. Jaiswal, P. Maity, S. Thakur, and M. Ripoll, Arxiv p. 2503.18099 (2025).
- [36] L. Harnau, R. G. Winkler, and P. Reineker, The Journal of chemical physics **102**, 7750 (1995).
- [37] T. Eisenstecken, G. Gompper, and R. G. Winkler, Polymers **8** (2016).
- [38] A. P. Thompson, H. M. Aktulga, R. Berger, D. S. Bolintineanu, W. M. Brown, P. S. Crozier, P. J. In't Veld, A. Kohlmeyer, S. G. Moore, T. D. Nguyen, et al., Computer physics communications **271**, 108171 (2022).
- [39] M. Fazelzadeh, E. Irani, Z. Mokhtari, and S. Jabbari-Farouji, Phys. Rev. E **108**, 024606 (2023).
- [40] E. Locatelli, V. Bianco, and P. Magaretti, Phys. Rev. Lett. **126**, 097801 (2021).
- [41] D. Breoni, E. Locatelli, and L. Tubiana, Macromolecules **58**, 10677 (2025).
- [42] J. P. Miranda-Lopez, E. Locatelli, C. Micheletti, D. Levis, and C. Valeriani, Journal of Chemical Theory and Computation **21**, 11910 (2025).

## Appendix A: Details on the analytical expansions

### 1. Analytical Expansions I: small active forces

Our strategy for tackling Eq. (22) analytically consists of a systematic expansion of all modes at small values of  $f^a$ .

In order to calculate  $\langle \mathbf{r}_i(t) \cdot \mathbf{r}_j \rangle$  at the different orders in  $f^a$  we need to calculate  $\langle \mathbf{r}_i(t) \cdot \boldsymbol{\eta}_j \rangle$ . We will employ the formal solution of  $\mathbf{r}_i(t)$ , obtained integrating Eq. (1) in its eigenfunction representation: it reads:

$$\mathbf{r}_i(t) = \int_0^t e^{-\frac{\Gamma_{ii}}{2}(t-\tau)} \left[ \mu \sum_m f_m \int_{-\frac{N}{2}}^{\frac{N}{2}} \frac{\sum_{n \neq i} \psi_m(s) \partial_s \psi_n(s) \mathbf{r}_n(\tau)}{\sqrt{\langle \Theta(s) \rangle}} \psi_i(s) ds + \boldsymbol{\eta}_i(\tau) \right] d\tau. \quad (\text{A1})$$

In order to simplify the notation we introduce the steady state expectation value expansion of  $\langle \Theta(s) \rangle$  up to second order in  $f^a$

$$\langle \Theta(s) \rangle = \langle \Theta(s) \rangle_0 + \langle \Theta(s) \rangle_1 + \langle \Theta(s) \rangle_2. \quad (\text{A2})$$

*a. Zeroth order* At zeroth order in  $f^a$ , using Eqs. (9), (A1), we obtain:

$$\langle \boldsymbol{\eta}_j \cdot \mathbf{r}_i \rangle_0^\infty = \langle \boldsymbol{\eta}_j \cdot \mathbf{r}_i^{(0)} \rangle_0^\infty = \lim_{t \rightarrow \infty} \int_0^t e^{-\frac{\Gamma_{ii}^{(0)}}{2}(t-\tau)} \langle \boldsymbol{\eta}_i(\tau) \cdot \boldsymbol{\eta}_j(t) \rangle d\tau = \delta_{ij} 2d\mu k_B T \quad (\text{A3})$$

where  $\mathbf{r}_i^{(0)}(t)$  is the zeroth-order solution obtained from Eq. (A1) and  $d$  is the dimension of the space in which the polymer is embedded in. Hence we have

$$\langle \mathbf{r}_i \cdot \mathbf{r}_j \rangle_0^\infty = \lim_{t \rightarrow \infty} \int_0^t \int_0^t e^{-\frac{\Gamma_{ii}^{(0)}}{2}(t-\tau_1)} e^{-\frac{\Gamma_{jj}^{(0)}}{2}(t-\tau)} \delta_{ij} \langle \boldsymbol{\eta}_i(\tau_1) \cdot \boldsymbol{\eta}_j(\tau) \rangle d\tau d\tau_1 = \delta_{ij} d \frac{\mu k_B T}{\zeta_i} \quad (\text{A4})$$

where  $\Gamma_{ii}^{(0)} = 2\zeta_i = 2\mu k_i^2 (Gk_i^2 + D)$  is the zeroth order contribution in  $f^a$  to  $\Gamma_{ii}$ . For later use we note that

$$\langle \Theta(s) \rangle_0 = \sum_n \sum_m \partial_s \psi_n(s) \partial_s \psi_m(s) \langle \mathbf{r}_n \cdot \mathbf{r}_n \rangle_0^\infty = \sum_n (\partial_s \psi_n(s))^2 \langle \mathbf{r}_n(t) \cdot \mathbf{r}_n(t) \rangle_0^\infty \quad (\text{A5})$$

Hence, since all  $\psi(s)$  have a definite parity then  $\langle \Theta(s, t) \rangle_0$  is an even function in the interval  $-N/2 < s < N/2$ .

*b. First order* At first order, using the same mean-field approximation introduced in Sec. IIB we have

$$\begin{aligned} \langle \boldsymbol{\eta}_j(t) \cdot \mathbf{r}_i(t) \rangle_1 &= \mu \sum_m f_m \int_{-\frac{N}{2}}^{\frac{N}{2}} \int_0^t \sum_{n \neq i} e^{-\frac{\Gamma_{ii}^{(0)}}{2}(t-\tau)} \frac{\psi_m(s) \psi_i(s) \partial_s \psi_n(s)}{\sqrt{\langle \Theta(s) \rangle_0}} \langle \boldsymbol{\eta}_j(t) \cdot \mathbf{r}_n(\tau) \rangle_0 d\tau ds + \\ &\quad - \int_0^t e^{-\frac{\Gamma_{ii}^{(0)}}{2}(t-\tau)} \frac{\Gamma_{ii}^{(1)}(t-\tau)}{\Gamma_{ii}^{(0)}} \langle \boldsymbol{\eta}_j(t) \cdot \boldsymbol{\eta}_i(\tau) \rangle_0 d\tau \end{aligned} \quad (\text{A6})$$

where

$$\Gamma_{ij}^{(1)} = -\mu \sum_m f_m \int_{-\frac{N}{2}}^{\frac{N}{2}} \frac{\psi_m(s)\psi_i(s)\partial_s\psi_i(s) + \psi_m(s)\psi_j(s)\partial_s\psi_j(s)}{\sqrt{\langle\Theta(s,t)\rangle_0}} ds \quad (\text{A7})$$

is the first order contribution of  $\Gamma_{ij}$  (see Eq. (23)). We highlight that the following equalities hold at  $t \rightarrow \infty$ :

$$\int_0^t e^{-\frac{\Gamma_{ij}^{(0)}}{2}(t-\tau)} \langle \boldsymbol{\eta}_j(t) \cdot \mathbf{r}_n(\tau) \rangle_0 d\tau = \int_0^t e^{-\frac{\Gamma_{ij}^{(0)}}{2}(t-\tau)} \int_0^\tau e^{-\frac{\Gamma_{ij}^{(0)}}{2}(\tau-\tau_1)} \langle \boldsymbol{\eta}_j(t) \cdot \boldsymbol{\eta}_n(\tau_1) \rangle_0 d\tau_1 d\tau = 0 \quad (\text{A8})$$

where we used the result Eq. (A3), and

$$\int_0^t e^{-\frac{\Gamma_{ij}^{(0)}}{2}(t-\tau)} \frac{\Gamma_{ii}^{(1)}(t-\tau)}{\Gamma_{ii}^{(0)}} \langle \boldsymbol{\eta}_j(t) \cdot \boldsymbol{\eta}_i(\tau) \rangle_0 d\tau = 0; \quad (\text{A9})$$

both equalities are using the fact that  $\boldsymbol{\eta}$  is a white noise. Using these results Eq. (A6) reads

$$\langle \boldsymbol{\eta}_j(t) \cdot \mathbf{r}_i(t) \rangle_1 = \langle \boldsymbol{\eta}_i(t) \cdot \mathbf{r}_j(t) \rangle_1 = 0 \quad (\text{A10})$$

from which we obtain

$$\begin{aligned} \langle \mathbf{r}_i \cdot \mathbf{r}_j \rangle_1^\infty &= \mu \sum_m f_m \int_{-\frac{N}{2}}^{\frac{N}{2}} \psi_m(s) \frac{\sum_{n \neq i} \psi_i(k_i s) \partial_s \psi_n(s) \langle \mathbf{r}_n \cdot \mathbf{r}_j \rangle_0^\infty + \sum_{n \neq j} \psi_j(s) \partial_s \psi_n(s) \langle \mathbf{r}_i \cdot \mathbf{r}_n \rangle_0^\infty}{\Gamma_{ij}^{(0)} \sqrt{\langle \Theta(s) \rangle_0}} ds \\ &= \frac{\mu}{\Gamma_{ij}^{(0)}} (1 - \delta_{ij}) d \sum_m f_m \left[ \frac{\mu k_B T}{\zeta_j} \xi_{ijm}^{(0)} + \frac{\mu k_B T}{\zeta_i} \xi_{jim}^{(0)} \right] \end{aligned} \quad (\text{A11})$$

where the term  $1 - \delta_{ij}$  stems from the constraints on the sums. We used Eq. (A4) to obtain the second line; we introduce

$$\xi_{ijm}^{(0)} = \int_{-\frac{N}{2}}^{\frac{N}{2}} \frac{\psi_m(s)\psi_i(s)\partial_s\psi_j(s)}{\sqrt{\langle\Theta(s)\rangle_0}} ds \quad (\text{A12})$$

*c. Second order* At second order, using again the same mean-field approximation we obtain

$$\begin{aligned} \langle \boldsymbol{\eta}_j(t) \cdot \mathbf{r}_i^{(2)}(t) \rangle &= \int_0^t \mu \sum_m f_m \int_{-\frac{N}{2}}^{\frac{N}{2}} e^{-\frac{\Gamma_{ij}^{(0)}}{2}(t-\tau)} \left[ \frac{\sum_{n \neq i} \langle \boldsymbol{\eta}_j(t) \mathbf{r}_n^{(1)}(\tau) \rangle \psi_m(s)\psi_i(s)\partial_s\psi_n(s)}{\sqrt{\langle \Theta(s) \rangle_0}} \right] ds d\tau + \\ &\quad - \int_0^t \frac{\mu f^a}{2} \int_{-\frac{N}{2}}^{\frac{N}{2}} e^{-\frac{\Gamma_{ij}^{(0)}}{2}(t-\tau)} \left[ \frac{\sum_{n \neq i} \langle \boldsymbol{\eta}_j(t) \mathbf{r}_n(\tau) \rangle_0 \psi_m(s)\psi_i(s)\partial_s\psi_n(s) \langle \Theta(s) \rangle_1}{\sqrt{\langle \Theta(s) \rangle_0} \langle \Theta(s) \rangle_0} \right] ds d\tau + \\ &\quad + \int_0^t \frac{\mu f^a}{2} \int_{-\frac{N}{2}}^{\frac{N}{2}} e^{-\frac{\Gamma_{ij}^{(0)}}{2}(t-\tau)} \frac{\Gamma_{ii}^{(1)}(t-\tau)}{\Gamma_{ii}^{(0)}} \left[ \frac{\sum_{n \neq i} \langle \boldsymbol{\eta}_j(t) \mathbf{r}_n^{(0)}(\tau) \rangle \psi_m(s)\psi_i(s)\partial_s\psi_n(s)}{\sqrt{\langle \Theta(s) \rangle_0}} \right] ds d\tau + \\ &\quad + \int_0^t e^{-\frac{\Gamma_{ij}^{(0)}}{2}(t-\tau)} \frac{\Gamma_{ii}^{(2)}(t-\tau)}{\Gamma_{ii}^{(0)}} \langle \boldsymbol{\eta}_j(t) \cdot \boldsymbol{\eta}_i(\tau) \rangle_0 d\tau \\ &= 0 \end{aligned} \quad (\text{A13})$$

We note that the first and second terms of Eq. (A13) vanish due to Eq. (A8), the third and fourth terms of Eq. (A13) vanish due to Eq. (A9). Finally, using Eq. (A10) we have:

$$\begin{aligned}
\langle \mathbf{r}_i \cdot \mathbf{r}_j \rangle_2^\infty &= \frac{\mu}{\Gamma_{ij}^{(0)}} \sum_m f_m \left[ \sum_{n \neq i} \langle \mathbf{r}_j \cdot \mathbf{r}_n \rangle_1^\infty \xi_{inm}^{(0)} + \sum_{n \neq j} \langle \mathbf{r}_i \cdot \mathbf{r}_n \rangle_1^\infty \xi_{jnm}^{(0)} \right] + \\
&- \frac{\mu}{\Gamma_{ij}^{(0)}} \sum_m f_m \left[ \sum_{n \neq i} \langle \mathbf{r}_j \cdot \mathbf{r}_n \rangle_0^\infty \xi_{inm}^{(0)} + \sum_{n \neq j} \langle \mathbf{r}_i \cdot \mathbf{r}_n \rangle_0^\infty \xi_{jnm}^{(0)} \right] \frac{\Gamma_{ij}^{(1)}}{\Gamma_{ij}^{(0)}} + \\
&+ \frac{\mu}{2\Gamma_{ij}^{(0)}} \sum_m f_m \left[ \sum_{n \neq i} \langle \mathbf{r}_j \cdot \mathbf{r}_n \rangle_0^\infty \xi_{inm}^{(1)} + \sum_{n \neq j} \langle \mathbf{r}_i \cdot \mathbf{r}_n \rangle_0^\infty \xi_{jnm}^{(1)} \right] + \\
&- \frac{1}{2\Gamma_{ij}^{(0)}} \left[ \frac{\Gamma_{ij}^{(2)}}{\Gamma_{ij}^{(0)}} (\langle \boldsymbol{\eta}_j \cdot \boldsymbol{\eta}_i \rangle_0^\infty + \langle \boldsymbol{\eta}_i \cdot \boldsymbol{\eta}_j \rangle_0^\infty) \right]
\end{aligned} \tag{A14}$$

where

$$\Gamma_{ij}^{(2)} = -\mu \sum_m f_m (\xi_{im}^{(1)} + \xi_{jm}^{(1)}) \tag{A15}$$

$$\xi_{ijm}^{(1)} = \int_{-\frac{N}{2}}^{\frac{N}{2}} \frac{\psi_m(s) \psi_i(s) \partial_s \psi_j(s) \langle \Theta(s) \rangle_1}{\sqrt{\langle \Theta(s) \rangle_0} \langle \Theta(s) \rangle_0} ds \tag{A16}$$

Using Eqs. (9), (A4) we obtain:

$$\begin{aligned}
\langle \mathbf{r}_i \cdot \mathbf{r}_j \rangle_2^\infty &= \frac{\mu}{\Gamma_{ij}^{(0)}} \sum_m f_m \left[ \sum_{n \neq i} \langle \mathbf{r}_j \cdot \mathbf{r}_n \rangle_1^\infty \xi_{inm}^{(0)} + \sum_{n \neq j} \langle \mathbf{r}_i \cdot \mathbf{r}_n \rangle_1^\infty \xi_{jnm}^{(0)} \right] + \\
&+ (1 - \delta_{ij}) \frac{d\mu^2 k_B T}{2\Gamma_{ij}^{(0)}} \sum_m f_m \left[ \frac{\xi_{ijm}^{(1)}}{\zeta_j} + \frac{\xi_{jim}^{(1)}}{\zeta_i} \right] - d\mu k_B T \delta_{ij} \frac{\Gamma_{ij}^{(2)}}{(\Gamma_{ij}^{(0)})^2}
\end{aligned} \tag{A17}$$

where the  $1 - \delta_{ij}$  stems from the restriction on the sum on the second line of Eq.(A14).

## 2. Analytical Expansion II: Short persistence length

In order to calculate the last expression we assume that the persistence length is small,  $l_p \ll N$ . As reported in the main text, in this regime we have that  $\beta_n^2 = k_n^2 + 1/l_p^2 \gg N$ : the hyperbolic functions are of order unity only in the close vicinity of the edges of the polymer and we approximate  $k_n = \pi n/N$ ,  $\beta_n \rightarrow \infty$ . Shifting the domain of definition of the variable  $s$ , we obtain the eigenfunctions Eqs. 27. Moreover we rewrite the eigenvalues as

$$\zeta_i = \mu k_i^2 (G k_i^2 + D) = \mu i^2 \frac{D \pi^2}{N^2} (\Lambda_p i^2 + 1), \quad \Lambda_p = \frac{l_p^2 \pi^2}{N^2} \tag{A18}$$

*a. Zeroth order* Defining  $\bar{z}_n = n^2(1 + \Lambda_p n^2)$  and using the definitions of  $Q$  and  $\Lambda_p$ , Eqs. (A18) at zeroth order we have:

$$\Gamma_{ij}^{(0)} = \frac{\pi^2 \mu D}{N^2} (\bar{z}_i + \bar{z}_j) \tag{A19}$$

$$\langle \mathbf{r}_i \cdot \mathbf{r}_j \rangle_0^\infty = \delta_{ij} d \frac{k_B T N^2}{\pi^2 D} \frac{1}{\bar{z}_i} \tag{A20}$$

$$\langle \Theta(s) \rangle_0 = 2d \frac{k_B T}{ND} \sum_{n=0}^{\infty} n^2 \frac{\sin^2(k_n s)}{\bar{z}_n} \tag{A21}$$

Eq. (A20) corresponds to Eq. (30a) of the main text. The expression in Eq. (A21) can be rewritten in terms of hypergeometric functions. Numerical inspection of Eq. (A21) in the regime  $\Lambda_p \ll N$  shows that

$$\sum_{n=0}^{\infty} n^2 \frac{\sin^2(k_n s)}{\bar{z}_n} \simeq \frac{\pi}{4} \frac{1}{\sqrt{\Lambda_p}} \frac{\cosh[\kappa N/2] - \cosh[\kappa(s - N/2)]}{\cosh[\kappa N/2] - 1} \quad (\text{A22})$$

with  $\kappa \simeq \frac{1}{N} 2\pi/\sqrt{\Lambda_p} \equiv 2/l_p$ ; when  $\kappa N \gg 1$  we can approximate

$$\sum_{n=0}^{\infty} n^2 \frac{\sin^2(k_n s)}{\bar{z}_n} \simeq \frac{\pi}{4} \frac{1}{\sqrt{\Lambda_p}} \quad (\text{A23})$$

i.e., with the value it attains at its maximum. Accordingly, using Eq. (4) we have

$$\langle \Theta(s) \rangle_0 \simeq \frac{d}{2} \frac{k_B T}{D l_p} = b^2 \quad (\text{A24})$$

$$\xi_{inm}^{(0)} \simeq - \left( \frac{2}{N} \right)^{\frac{3}{2}} \frac{1}{b} \int_0^N \frac{\pi n}{N} \sin(k_n s) \cos(k_i s) \cos(k_m s) ds \simeq - \left( \frac{2}{N} \right)^{\frac{3}{2}} \frac{1}{b} \bar{\xi}_{inm}^{(0)} \quad (\text{A25})$$

where we defined

$$\begin{aligned} \bar{\xi}_{inm}^{(0)} &= \frac{\pi n}{N} \int_0^N \sin(k_n s) \cos(k_i s) \cos(k_m s) ds \\ &= \frac{n^2 ((-1)^{i+m+n} - 1) (i^2 + m^2 - n^2)}{(i - m - n)(i + m - n)(i - m + n)(i + m + n)} \end{aligned} \quad (\text{A26})$$

*b. First order* Using the definitions of  $Q$  and  $\Lambda_p$ , Eqs. (A18) together with (A19), (A25) Eq. (A11), (A28) and Eq. (A16) respectively read

$$\langle \mathbf{r}_n \cdot \mathbf{r}_m \rangle_1^\infty = -8\sqrt{2} \frac{b^2 N^2}{\pi^4 d^2} \frac{1}{l_p^2} \frac{(1 - \delta_{nm})}{\bar{z}_n + \bar{z}_m} \sum_l \frac{f_l b \sqrt{N}}{k_B T} \left( \frac{\bar{\xi}_{nml}^{(0)}}{\bar{z}_m} + \frac{\bar{\xi}_{mnl}^{(0)}}{\bar{z}_n} \right) \quad (\text{A27})$$

$$\langle \Theta(s) \rangle_1 = \frac{2}{N} \sum_n \sum_m k_n k_m \sin(k_n s) \sin(k_m s) \langle \mathbf{r}_n \cdot \mathbf{r}_m \rangle_1^\infty \quad (\text{A28})$$

and hence

$$\xi_{ijr}^{(1)} \simeq \left( \frac{2}{N} \right)^{\frac{5}{2}} \frac{1}{b^3} \sum_n \sum_m \langle \mathbf{r}_n \cdot \mathbf{r}_m \rangle_1^\infty \int_0^N \frac{\pi^3 j \cdot n \cdot m}{N^3} \cos(k_r s) \cos(k_i s) \sin(k_j s) \sin(k_n s) \sin(k_m s) ds \quad (\text{A29})$$

$$\simeq - \frac{4}{\pi^2 l_p^2} \frac{1}{N^{\frac{5}{2}}} \frac{1}{b} \sum_n \sum_m (1 - \delta_{nm}) \frac{j \cdot n \cdot m}{\bar{z}_n + \bar{z}_m} \sum_l \frac{f_l b \sqrt{N}}{k_B T} \left( \frac{\bar{\xi}_{nml}^{(0)}}{\bar{z}_m} + \frac{\bar{\xi}_{mnl}^{(0)}}{\bar{z}_n} \right) A_{ijmnr} \quad (\text{A30})$$

$$\simeq - \frac{4}{\pi^2 l_p^2} \frac{1}{N^{\frac{5}{2}}} \frac{1}{b} \bar{\xi}_{ijr}^{(1)} \quad (\text{A31})$$

with

$$\bar{\xi}_{ijr}^{(1)} = \sum_l \frac{f_l b \sqrt{N}}{k_B T} \sum_n \sum_m (1 - \delta_{nm}) \frac{j \cdot n \cdot m}{\bar{z}_n + \bar{z}_m} \left( \frac{\bar{\xi}_{nml}^{(0)}}{\bar{z}_m} + \frac{\bar{\xi}_{mnl}^{(0)}}{\bar{z}_n} \right) A_{ijmnr} \quad (\text{A32})$$

$$A_{ijmnr} = \frac{16\pi}{N} \int_0^N \cos(k_r s) \cos(k_i s) \sin(k_j s) \sin(k_n s) \sin(k_m s) ds \quad (\text{A33})$$

*c. Second order* At second order, Eq. (A17) reads:

$$\begin{aligned} \langle \mathbf{r}_i \cdot \mathbf{r}_j \rangle_2^\infty &= \frac{64}{\pi^6} \frac{b^2 N^2}{l_p d^3} \frac{1}{\bar{z}_i + \bar{z}_j} \sum_m \frac{f_m b \sqrt{N}}{k_B T} \sum_l \frac{f_l b \sqrt{N}}{k_B T} \left[ \sum_{n \neq i} \frac{1 - \delta_{jn}}{\bar{z}_n + \bar{z}_j} \left( \frac{\bar{\xi}_{jnl}^{(0)}}{\bar{z}_n} + \frac{\bar{\xi}_{njl}^{(0)}}{\bar{z}_j} \right) \bar{\xi}_{inm}^{(0)} + \sum_{n \neq j} \frac{1 - \delta_{in}}{\bar{z}_n + \bar{z}_i} \left( \frac{\bar{\xi}_{sinl}^{(0)}}{\bar{z}_n} + \frac{\bar{\xi}_{snl}^{(0)}}{\bar{z}_i} \right) \bar{\xi}_{jnm}^{(0)} \right] + \\ &\quad - \frac{8b^2 N^2}{d\pi^6} \frac{1 - \delta_{ij}}{\bar{z}_i + \bar{z}_j} \sum_r \frac{f_r b \sqrt{N}}{k_B T} \left[ \frac{\bar{\xi}_{ijr}^{(1)}}{\bar{z}_j} + \frac{\bar{\xi}_{jir}^{(1)}}{\bar{z}_i} \right] - \delta_{ij} \frac{8b^2 N^2}{\pi^6 d} \frac{1}{\bar{z}_i^2} \sum_r \frac{f_r b \sqrt{N}}{k_B T} \bar{\xi}_{iir}^{(1)} \end{aligned} \quad (\text{A34})$$

That for diagonal terms becomes

$$\langle \mathbf{r}_i \cdot \mathbf{r}_j \rangle_2^\infty = \frac{64 b^2 N^2}{\pi^6} \frac{1}{l_p d^3} \frac{1}{\bar{z}_i} \sum_m \frac{f_m b \sqrt{N}}{k_B T} \sum_l \frac{f_l b \sqrt{N}}{k_B T} \left[ \sum_{n \neq i} \frac{1 - \delta_{in}}{\bar{z}_n + \bar{z}_i} \left( \frac{\bar{\xi}_{inl}^{(0)}}{\bar{z}_n} + \frac{\bar{\xi}_{nil}^{(0)}}{\bar{z}_i} \right) \bar{\xi}_{inm}^{(0)} \right] - \frac{8b^2 N^2}{\pi^6 d} \frac{1}{\bar{z}_i^2} \sum_r \frac{f_r b \sqrt{N}}{k_B T} \bar{\xi}_{iir}^{(1)} \quad (\text{A35})$$

### 3. Single force mode and relevant Péclet number

In the case of a single Fourier mode of the active force, by comparing the values of the correlation at zeroth order to those at first order we obtain that the latter are much smaller than the former when

$$\text{Pe}_l = \frac{f_l b \sqrt{N}}{k_B T} \ll 1, \quad (\text{A36})$$

which indeed has the form of a Péclet number. It is interesting to note that the Péclet number in Eq. (A36) scales as  $\sqrt{N}$ . For such a single-mode force, we can simplify the expression at first order

$$\langle \mathbf{r}_n \cdot \mathbf{r}_m \rangle_1^\infty = -8\sqrt{2} \frac{b^2 N^2}{\pi^4 d^2} \frac{1}{l_p^2} \frac{(1 - \delta_{nm})}{\bar{z}_n + \bar{z}_m} \sum_l \text{Pe}_l \left( \frac{\bar{\xi}_{nml}^{(0)}}{\bar{z}_m} + \frac{\bar{\xi}_{mnl}^{(0)}}{\bar{z}_n} \right), \quad (\text{A37})$$

as well as at second order

$$\begin{aligned} \langle \mathbf{r}_i \cdot \mathbf{r}_j \rangle_2^\infty &= \frac{64 b^2 N^2}{\pi^6} \frac{1}{l_p d^3} \frac{1}{\bar{z}_i + \bar{z}_j} \text{Pe}_l^2 \left[ \sum_{n \neq i} \frac{1 - \delta_{jn}}{\bar{z}_n + \bar{z}_j} \left( \frac{\bar{\xi}_{jnl}^{(0)}}{\bar{z}_n} + \frac{\bar{\xi}_{njl}^{(0)}}{\bar{z}_j} \right) \bar{\xi}_{inl}^{(0)} + \sum_{n \neq j} \frac{1 - \delta_{in}}{\bar{z}_n + \bar{z}_i} \left( \frac{\bar{\xi}_{inl}^{(0)}}{\bar{z}_n} + \frac{\bar{\xi}_{nil}^{(0)}}{\bar{z}_i} \right) \bar{\xi}_{jnl}^{(0)} \right] + \\ &\quad - \frac{8b^2 N^2}{d\pi^6} \frac{1 - \delta_{ij}}{\bar{z}_i + \bar{z}_j} \text{Pe}_l \left[ \frac{\bar{\xi}_{ijl}^{(1)}}{\bar{z}_j} + \frac{\bar{\xi}_{jil}^{(1)}}{\bar{z}_i} \right] - \delta_{ij} \frac{8b^2 N^2}{\pi^6 d} \frac{1}{\bar{z}_i^2} \text{Pe}_l \bar{\xi}_{iil}^{(1)} \end{aligned} \quad (\text{A38})$$

The two expressions Eqs. (A37), (A38) are equivalent to those in Eqs. 30.

### 4. Polymer length & stretching coefficient

In the continuum model the total length of the polymer is not fixed and the polymer can be stretched. Since for real polymers this is rarely the case, we have computed the corrections that should be added to the "stretching" parameter  $D$  (see Eq. (1)) in order to keep the length of the polymer fixed. In principle this may be important as highlighted in Ref. [36]. The average length of the polymer is defined as  $L = \left\langle \sum_{i=1}^{N-1} |\mathbf{r}_{i+1} - \mathbf{r}_i| \right\rangle$ , that in the continuum limit reads

$$L = \left\langle \int_0^N \sqrt{\left( \frac{\partial_s \mathbf{r}(t)}{\partial s} \right)^2} ds \right\rangle \quad (\text{A39})$$

By imposing the constancy of  $L$  we can derive the corrections to the effective stretching coefficient that should be accounted for in order to keep  $L$  constant

$$\bar{D} = D_0 + D_1 + D_2 \quad (\text{A40})$$

As shown in Appendix A 4,  $\bar{D}_1 = 0$  and the leading corrections are hence quadratic in the force. We report the ratio between the length  $L$ , computed using Eq. (A43) over the nominal value  $L_0 = Nb$ , as a function of the number of monomers  $N$  for different modes  $m$  in Fig. 9a. We observe that, in the current approximation, the polymer length is barely affected by the activity and it remains almost constant. In particular,  $L$  diminishes for  $m \leq 1$ . Instead, it increases for  $m \geq 2$  indicating that the presence of forces with alternating sign will induce a stretching of the chain.

Finally, we provide an analytical expansion of  $L(s)$ . The average length of the polymer is defined as

$L = \left\langle \sum_{i=1}^{N-1} |\mathbf{r}_{i+1} - \mathbf{r}_i| \right\rangle$ , that in the continuum limit reads

$$L = \left\langle \int_0^N \sqrt{\left( \frac{\partial_s \mathbf{r}(t)}{\partial s} \right)^2} ds \right\rangle \quad (\text{A41})$$

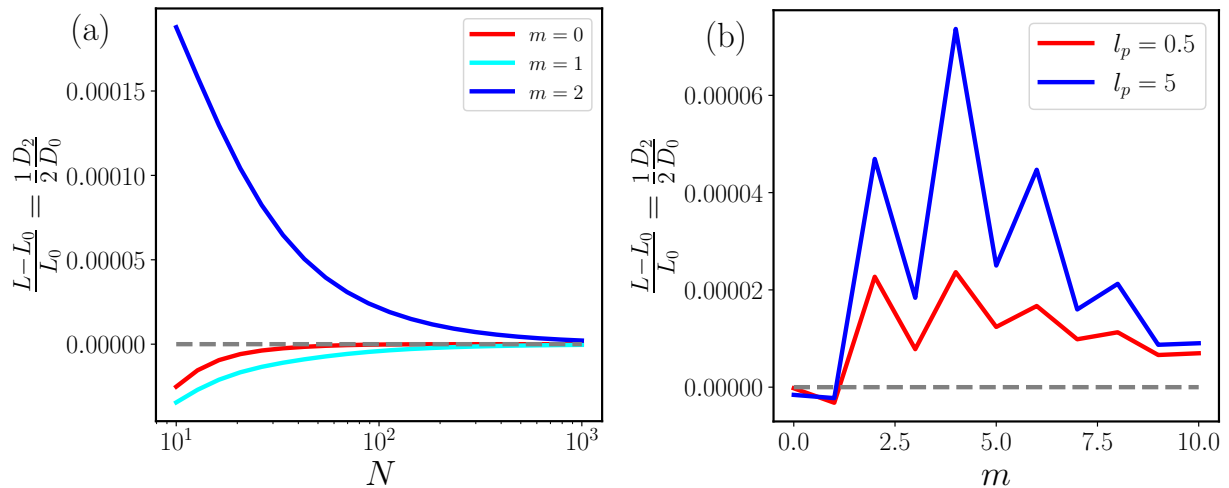


FIG. 9: (a): Elongation of the polymer  $(L - L_0)/L_0$  (with  $L_0 = Nb$ ) as function of  $N$  for a single-mode force for  $m = 0, 1, 2$  and for  $Pe_m = 1$ . We recall that due to Eqs. (A43),(A51) this is also equal to the normalized correction to the stretching coefficient  $D_2/D_0$ . (b): Elongation of the polymer  $(L - L_0)/L_0$  (with  $L_0 = Nb$ ) as function of the force mode for  $N = 100$ ,  $l_p = 0.5, 5$  as reported in the legend, and  $f_m = 1$ .

Using the eigenfunction representation, Eq. (A2) and the mean-field approximation we get:

$$L = \int_0^N \sqrt{\langle \Theta(s) \rangle_0} \left( 1 + \frac{1}{2} \frac{\langle \Theta(s) \rangle_1}{\langle \Theta(s) \rangle_0} + \frac{1}{2} \frac{\langle \Theta(s) \rangle_2}{\langle \Theta(s) \rangle_0} + \frac{1}{4} \left( \frac{\langle \Theta(s) \rangle_1}{\langle \Theta(s) \rangle_0} \right)^2 \right) ds \quad (\text{A42})$$

In particular,  $\langle \Theta(s) \rangle_0$  (see Eq. (A24)) does not depend on  $s$ , in the limit of small active forces and persistence length. The expression Eq. (A42) can be simplified

$$L = \sqrt{\frac{d k_B T}{2 D l_p}} \left[ N + \int_0^N \frac{1}{2} \frac{\langle \Theta(s) \rangle_2}{\langle \Theta(s) \rangle_0} + \frac{1}{4} \left( \frac{\langle \Theta(s) \rangle_1}{\langle \Theta(s) \rangle_0} \right)^2 ds \right] \quad (\text{A43})$$

as  $\int_0^N \langle \Theta(s) \rangle_1 ds = 0$ . The other two integrals in Eq. (A43) can be formally solved

$$\begin{aligned} \int_0^N \langle \Theta(s) \rangle_1^2 ds &= \frac{4d k_B T l_p N}{\pi^4 D^3} \mathcal{T}(\{f\}, l_p) \\ \int_0^N \langle \Theta(s) \rangle_2 ds &= \sum_n k_n^2 \langle \mathbf{r}_n \cdot \mathbf{r}_n \rangle_\infty^2 = \frac{2}{\pi^4} \frac{l_p N}{D^2} [4N \mathcal{W}(\{f\}, l_p) + 6l_p \mathcal{H}(\{f\}, l_p)] \end{aligned} \quad (\text{A44})$$

with

$$\mathcal{T}(\{f\}, l_p) = \sum_l f_l \sum_q f_q \sum_{i,j \neq i} \sum_{n,m \neq n} \left( \frac{\bar{\xi}_{nml}^{(0)}}{\bar{z}_m} + \frac{\bar{\xi}_{mnl}^{(0)}}{\bar{z}_n} \right) \frac{1}{\bar{z}_n + \bar{z}_m} \left( \frac{\bar{\xi}_{ijq}^{(0)}}{\bar{z}_j} + \frac{\bar{\xi}_{jiq}^{(0)}}{\bar{z}_i} \right) \frac{1}{\bar{z}_i + \bar{z}_j} (i \cdot j \cdot n \cdot m) \mathcal{L}_{ijnm} \quad (\text{A45})$$

$$\mathcal{L}_{ijnm} = \frac{8}{N} \int_0^N \sin(k_i s) \sin(k_j s) \sin(k_n s) \sin(k_m s) ds \quad (\text{A46})$$

$$\mathcal{W}(\{f\}, l_p) = \sum_n \sum_m \sum_{l \leq m} n^2 f_m f_l \bar{\chi}_{nml} \quad (\text{A47})$$

$$\mathcal{H}(\{f\}, l_p) = \sum_n \frac{1}{\bar{z}_n^2} \sum_m f_m \bar{\xi}_{nmm}^{(1)} \quad (\text{A48})$$

Note that  $\mathcal{L}_{ijnm} \neq 0$  only when  $\pm i \pm j \pm m \pm n = 0$ . It is also interesting to note that, at  $f^a = 0$  and using the definition of  $D$  Eq. (4), we retrieve the expected equilibrium value  $L = bN$ ; for  $f \neq 0$  the polymer becomes stretched

or compressed. However, since real polymers have a fixed contour length, we expand the stretching coefficient,  $D$ , in powers of  $f^a$  as  $D = D_0 + D_1 + D_2$  with

$$D_0 = \frac{d k_B T}{2 l_p b^2} \quad (\text{A49})$$

and defining  $D_1$  and  $D_2$  as those values for which  $\Delta L = L - bN = 0 + \mathcal{O}(f^3)$ . Accordingly we get

$$\bar{D}_1 = 0 \quad (\text{A50})$$

$$\bar{D}_2 = 2 \frac{D_0}{N} \int_0^N \frac{1}{2} \frac{\langle \Theta(s) \rangle_2}{\langle \Theta(s) \rangle_0} + \frac{1}{4} \left( \frac{\langle \Theta(s) \rangle_1}{\langle \Theta(s) \rangle_0} \right)^2 ds \quad (\text{A51})$$